

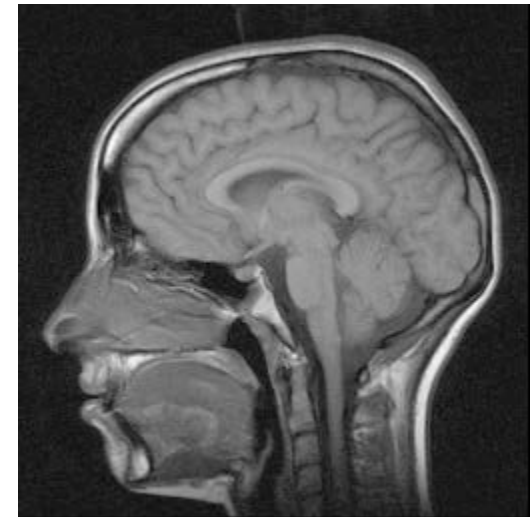
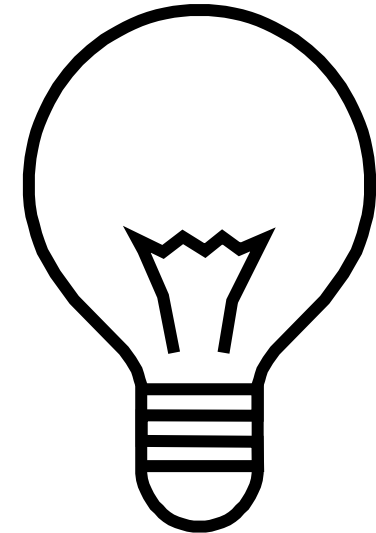


Oxford School on Neutron Scattering

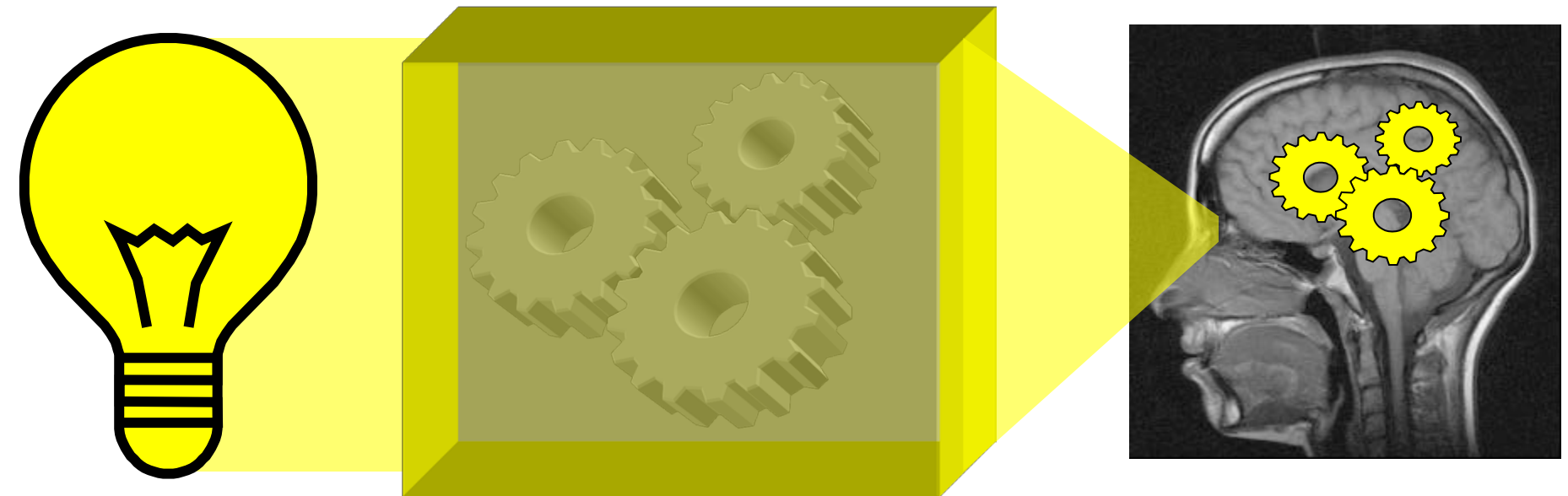
Neutron imaging

Nikolay Kardjilov

Neutron imaging



Neutron imaging



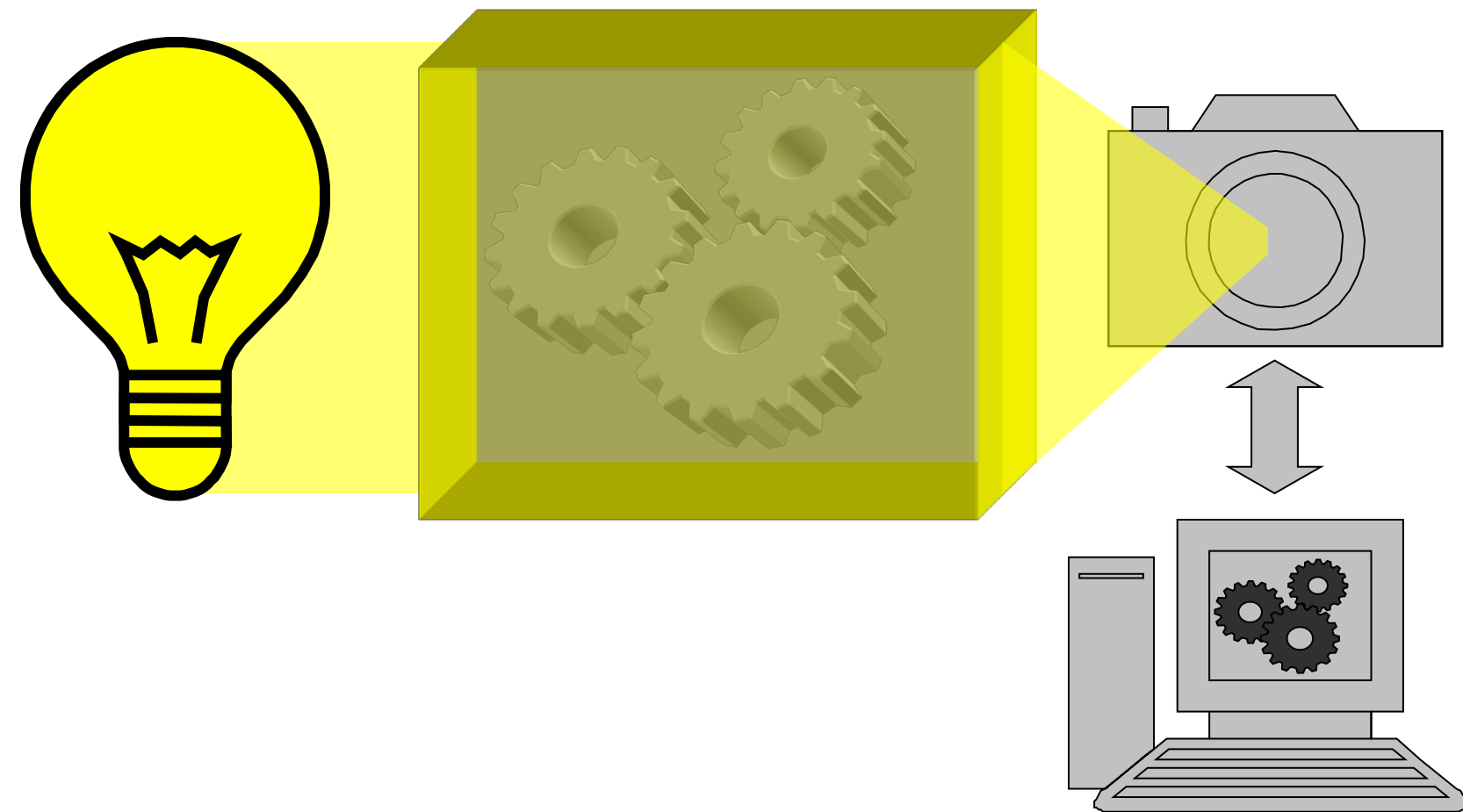


Neutron imaging

Source

Sample

Detector



Neutron imaging

Introduction



One of the first X-ray experiments late in 1895 performed by [Konrad Röntgen](#) was a film of a hand.

The bones and also finger rings deliver much higher contrast than the soft tissue.

Neutron imaging

Introduction

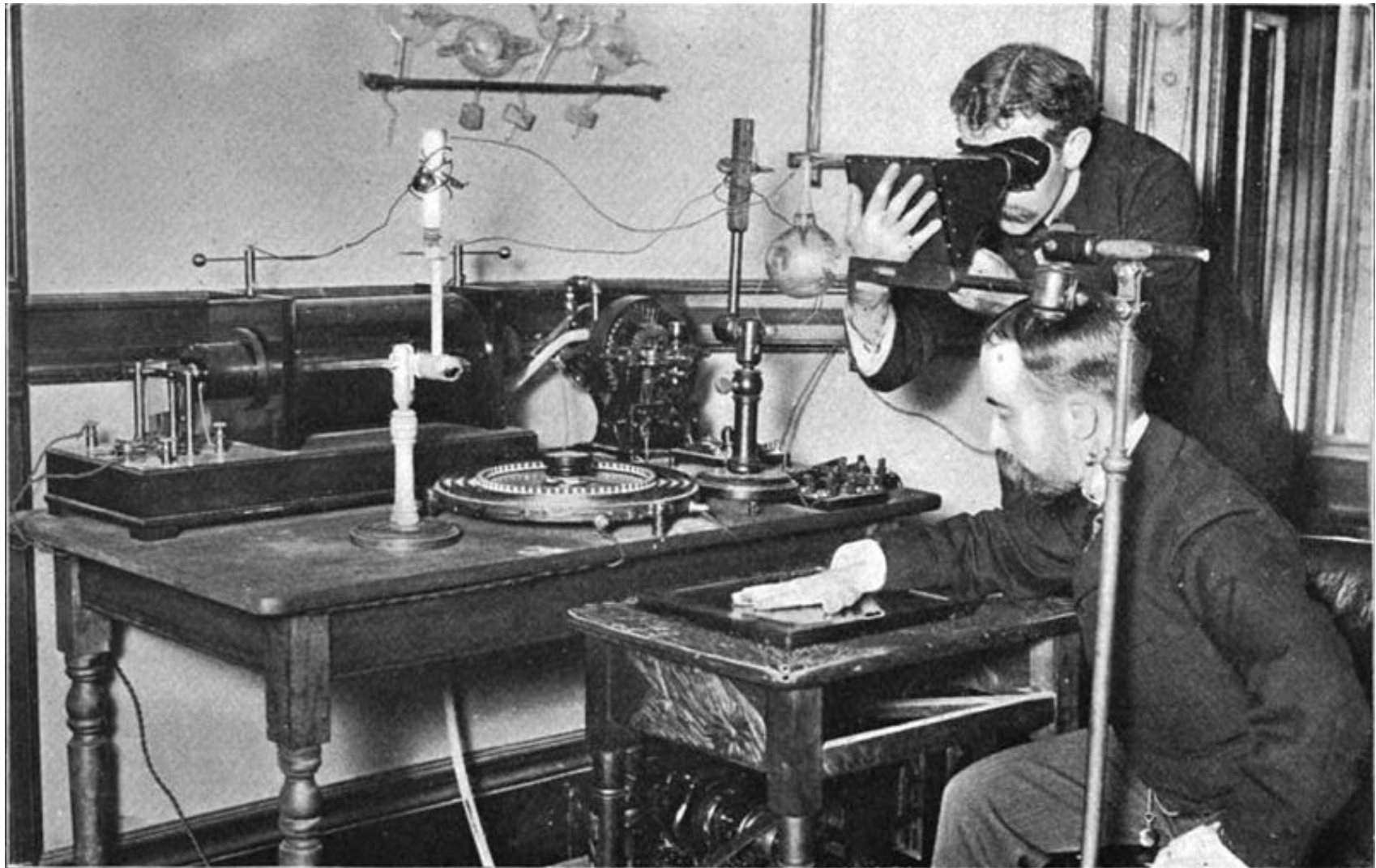


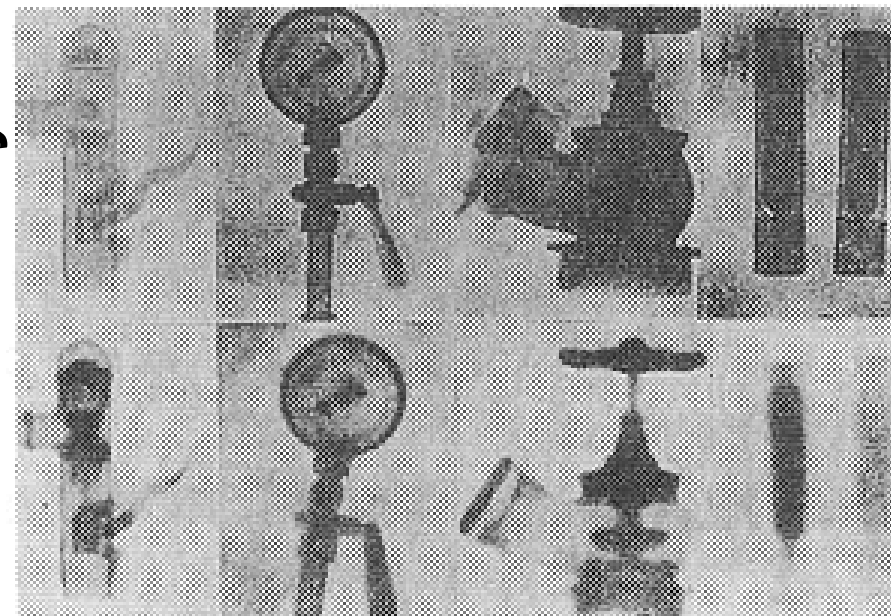
Photo of experimenters taking an X-ray with an early Crookes tube apparatus, from the late 1800s.



Neutron imaging

Roots of neutron radiography

x-rays
neutrons



Comparison between x-ray
and neutron images

Berlin, 1935 – 1938

H. Kallmann & Kuhn with Ra-Be
and neutron generator

Berlin until Dec. 1944

O. Peter with an
accelerator neutron source

But the real programs with neutrons started after World War II at research reactors



Neutron imaging

Introduction

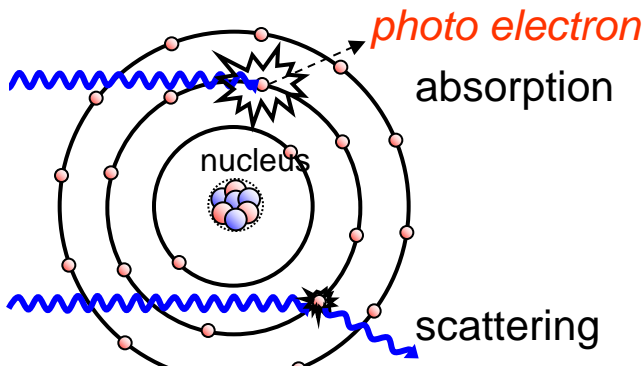


Sample image: X-ray showing frontal view of both hands.

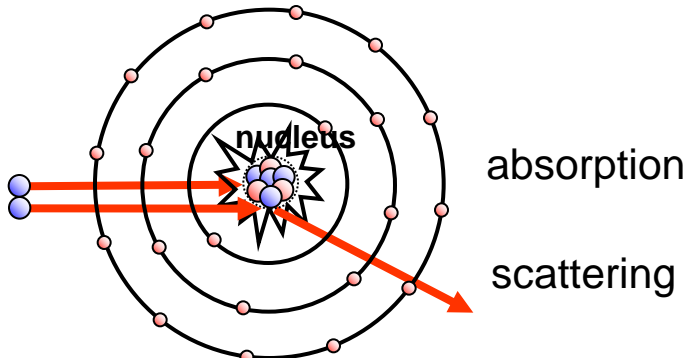
Neutron imaging

Neutron interaction with matter

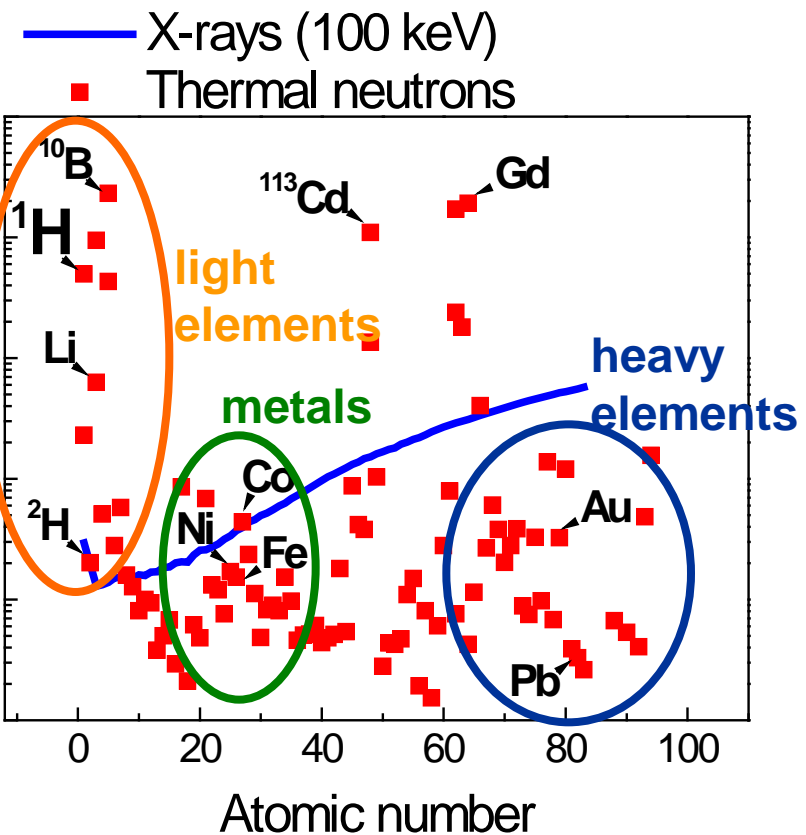
X-rays



neutrons



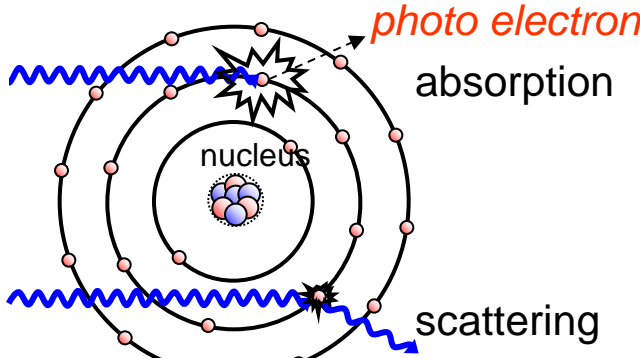
Mass attenuation coefficient, (cm^2/g)



Neutron imaging

Neutron interaction with matter

X-rays

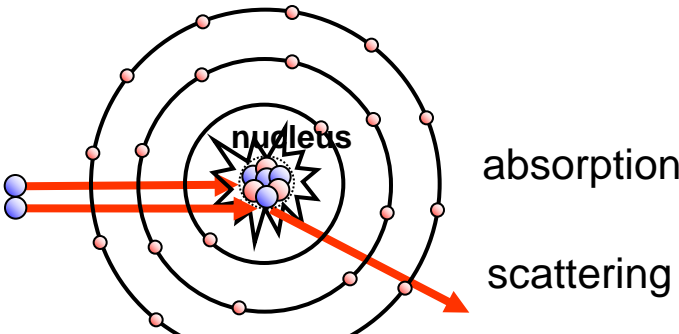


Attenuation coefficients with X-ray [cm⁻¹]

1a	2a	3b	4b	5b	6b	7b	8	1b	2b	3a	4a	5a	6a	7a	0		
H 0.02															He 0.02		
Li 0.06	Be 0.22														B 0.28		
Na 0.13	Mg 0.24														C 0.27		
K 0.14	Ca 0.26	Sc 0.48	Ti 0.73	V 1.04	Cr 1.29	Mn 1.32	Fe 1.57	Co 1.78	Ni 1.96	Cu 1.97	Zn 1.64	Ga 1.42	Ge 1.33	As 1.50	Se 1.23	Br 0.90	Kr 0.73
Rb 0.47	Sr 0.86	Y 1.61	Zr 2.47	Nb 3.43	Mo 4.29	Tc 5.06	Ru 5.71	Rh 6.08	Pd 6.13	Ag 5.67	Cd 4.84	In 4.31	Sn 3.98	Sb 4.28	Te 4.06	I 3.45	Xe 2.53
Cs 1.42	Ba 2.73	La 5.04	Hf 19.70	Ta 25.47	W 30.49	Re 34.47	Os 37.92	Ir 39.01	Pt 38.61	Au 35.94	Hg 25.88	Tl 23.23	Pb 22.81	Bi 20.28	Po 20.22	At 9.77	Rn
Fr	Ra 11.80	Ac 24.47	Rf	Ha													

Lanthanides	Ce 5.79	Pr 6.23	Nd 6.46	Pm 7.33	Sm 7.68	Eu 5.66	Gd 8.69	Tb 9.46	Dy 10.17	Ho 10.91	Er 11.70	Tm 12.49	Yb 9.32	Lu 14.07		
*Actinides	Th 28.95	Pa 39.65	U 49.08	Np	Pu	Am	Cm	Bk	Vf	Es	Fm	Md	No	Lr	x-ray	

neutrons



Attenuation coefficients with neutrons [cm⁻¹]

1a	2a	3b	4b	5b	6b	7b	8	1b	2b	3a	4a	5a	6a	7a	0		
H 3.44															He 0.02		
Li 3.30	Be 0.79														B 101.60		
Na 0.09	Mg 0.15														C 0.56		
K 0.06	Ca 0.08	Sc 2.00	Ti 0.60	V 0.72	Cr 0.54	Mn 1.21	Fe 1.19	Co 3.92	Ni 2.05	Cu 1.07	Zn 0.35	Ga 0.49	Ge 0.47	As 0.67	Se 0.73	Br 0.61	Kr 0.43
Rb 0.08	Sr 0.14	Y 0.27	Zr 0.29	Nb 0.40	Mo 0.52	Tc 1.76	Ru 0.58	Rh 10.88	Pd 0.78	Ag 4.04	Cd 115.11	In 7.58	Sn 0.21	Sb 0.30	Te 0.25	I 0.23	Xe 0.43
Cs 0.29	Ba 0.07	La 0.52	Hf 4.99	Ta 1.49	W 1.47	Re 6.85	Os 2.24	Ir 30.46	Pt 1.46	Au 6.23	Hg 16.21	Tl 0.47	Pb 0.38	Bi 0.27	Po At	Rn	
Fr	Ra 0.34	Ac	Rf	Ha													

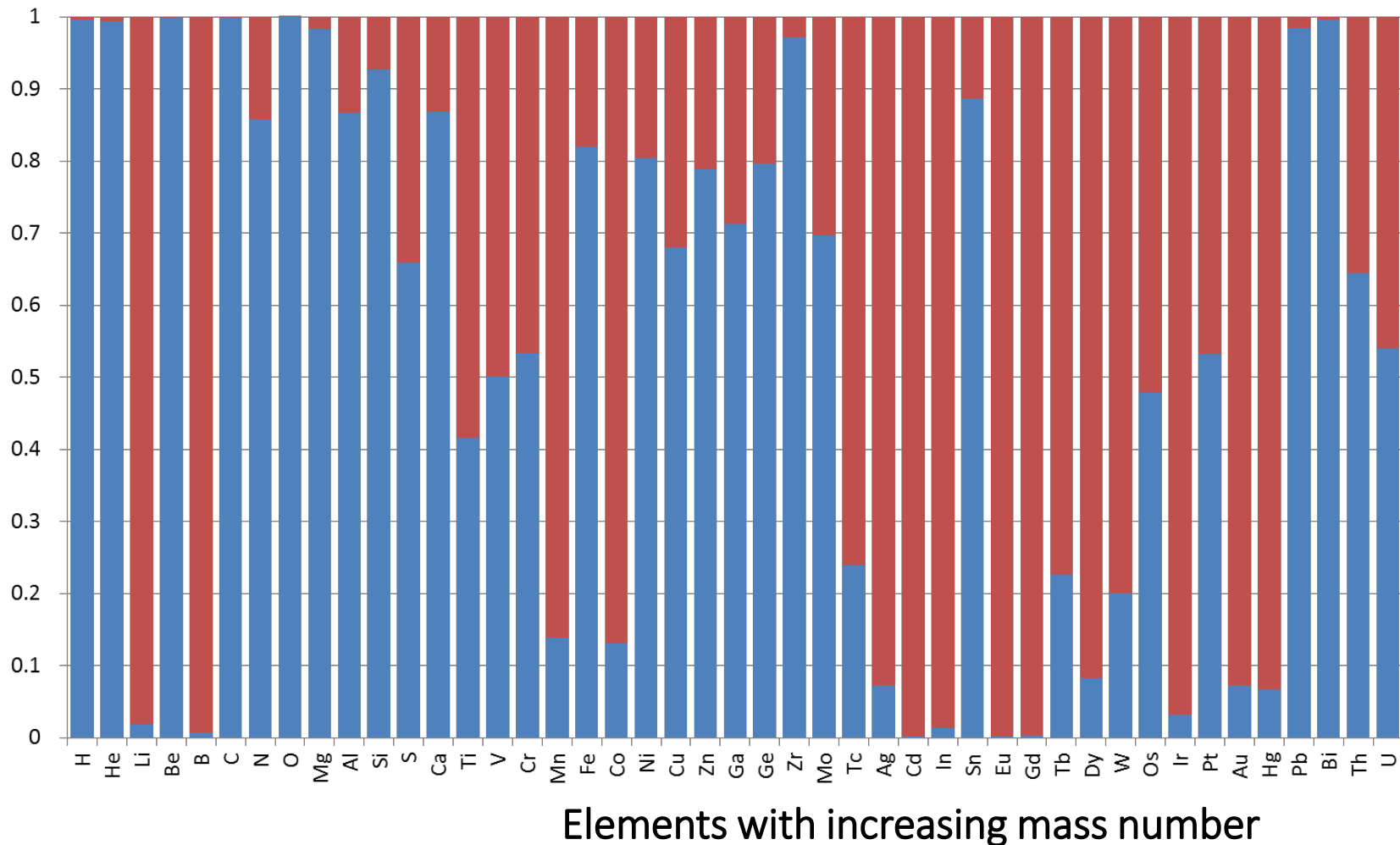
*Lanthanides	Ce 0.14	Pr 0.41	Nd 1.87	Pm 5.72	Sm 171.47	Eu 94.58	Gd 1479.04	Tb 0.93	Dy 32.42	Ho 2.25	Er 5.48	Tm 3.53	Yb 1.40	Lu 2.75		
**Actinides	Th 0.59	Pa 8.46	U 0.82	Np 9.80	Pu 50.20	Am 2.86	Cm	Bk	Cf	Es	Fm	Md	No	Lr	neut.	



Neutron imaging

Portion

- Normalized absorption cross section
- Normalized scattering cross section

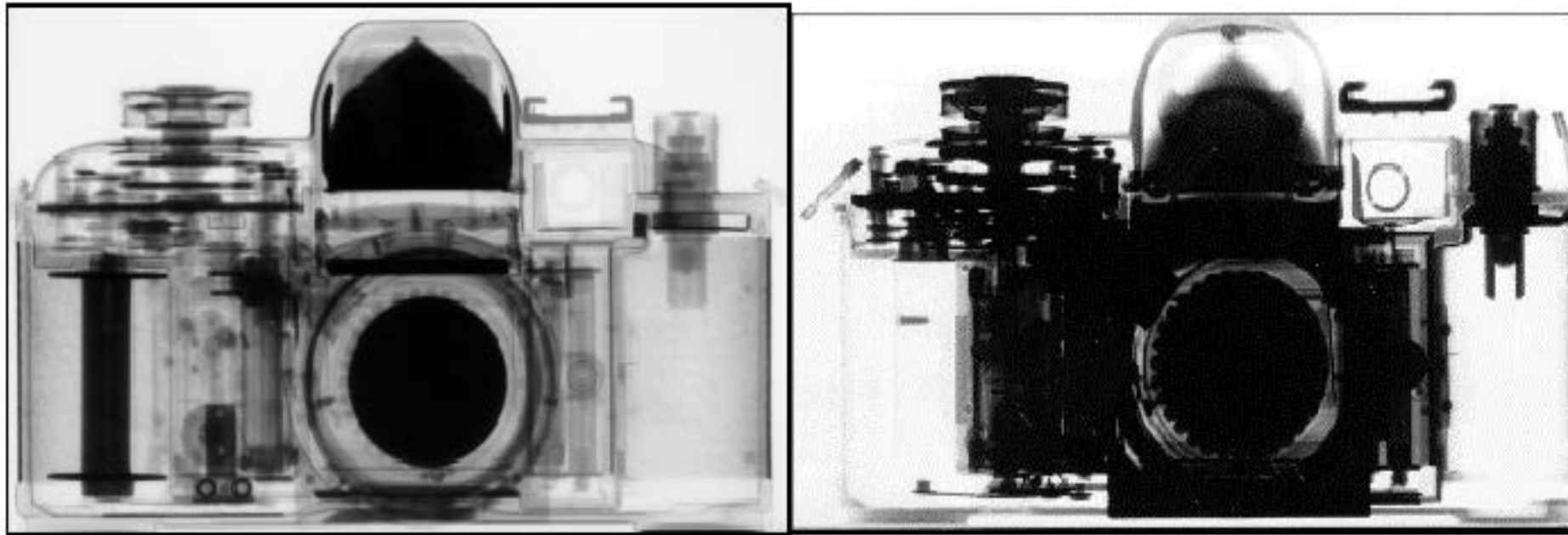


Elements with increasing mass number



Neutron imaging

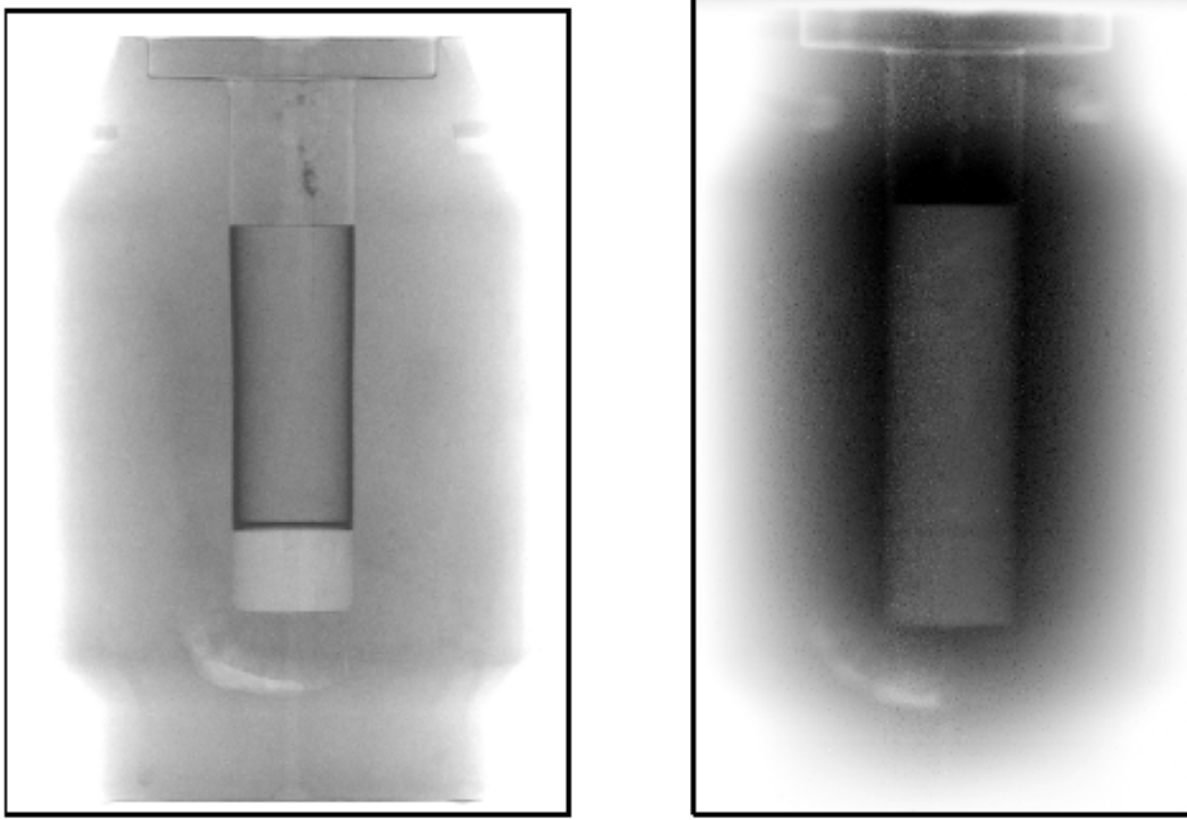
Neutron radiography - examples



The example for a camera helps to explain differences in neutron (left) and X-ray (right) radiography. Whereas the hydrogen containing parts can be visualised with neutron even at thin layers, thicker metallic components are hard to penetrate with X-rays.

Images courtesy: Dr. Eberhard Lehmann (Paul-Scherrer-Institute, Switzerland)

Neutron imaging



Observation of a lead container. The neutron image on the left was obtained after 20 s. On the right, the gamma radiography with Co-60 (1100 keV) needed 120 minutes of exposure.

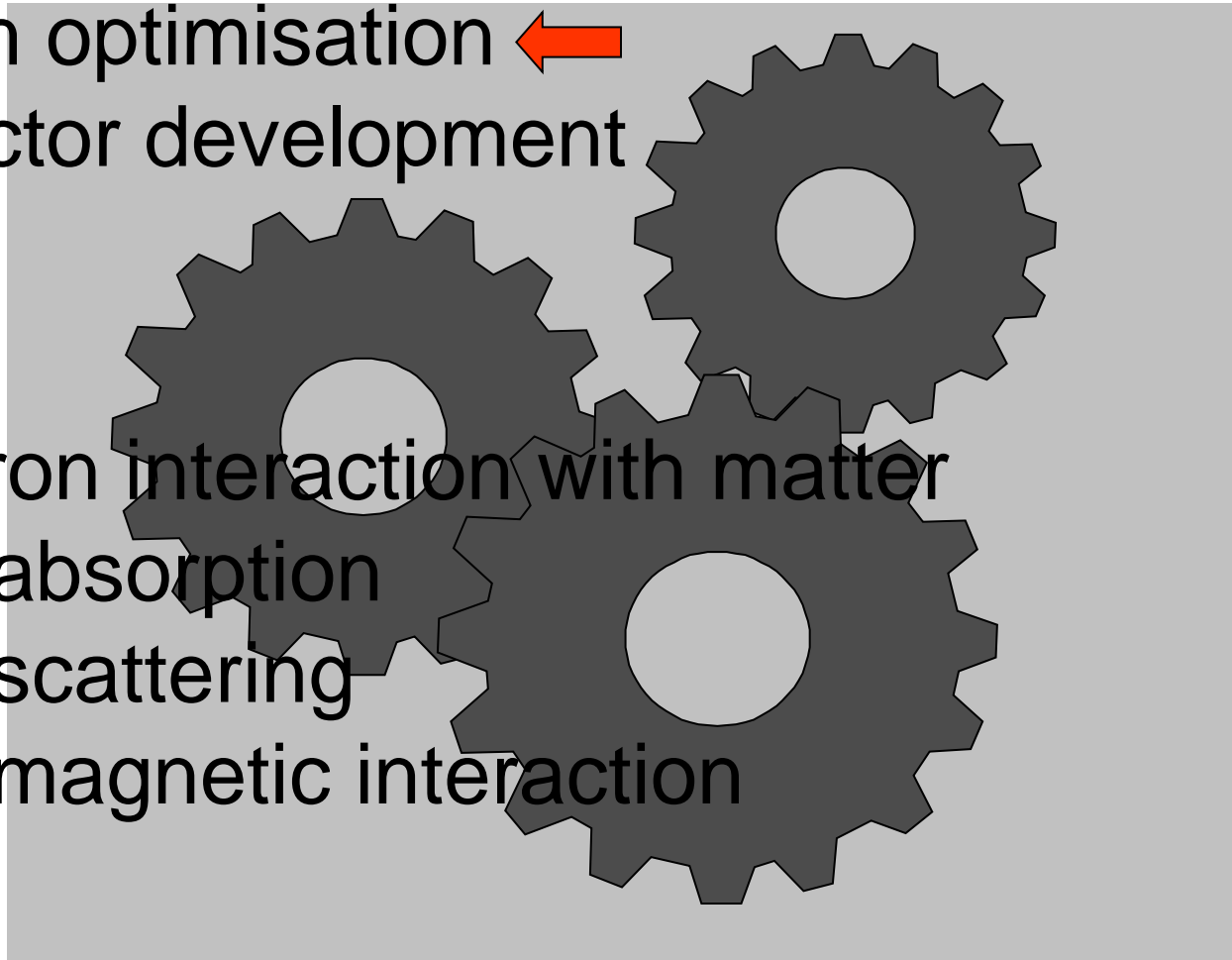
Images courtesy: Dr. Eberhard Lehmann (Paul-Scherrer-Institute, Switzerland)



Contrast

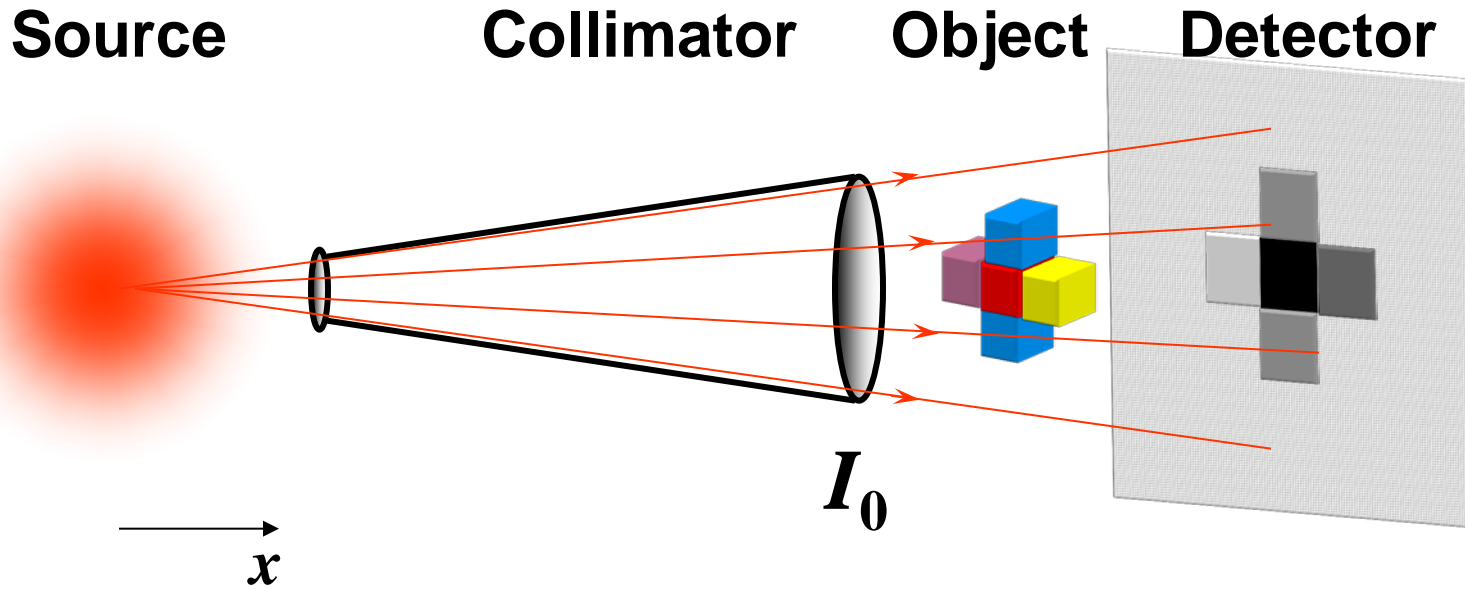
- Beam optimisation ←
- Detector development
- Neutron interaction with matter
 - absorption
 - scattering
 - magnetic interaction

Resolution





Beam optimisation



I_0

$$\sim I_0 e^{-\int \Sigma(x) dx}$$

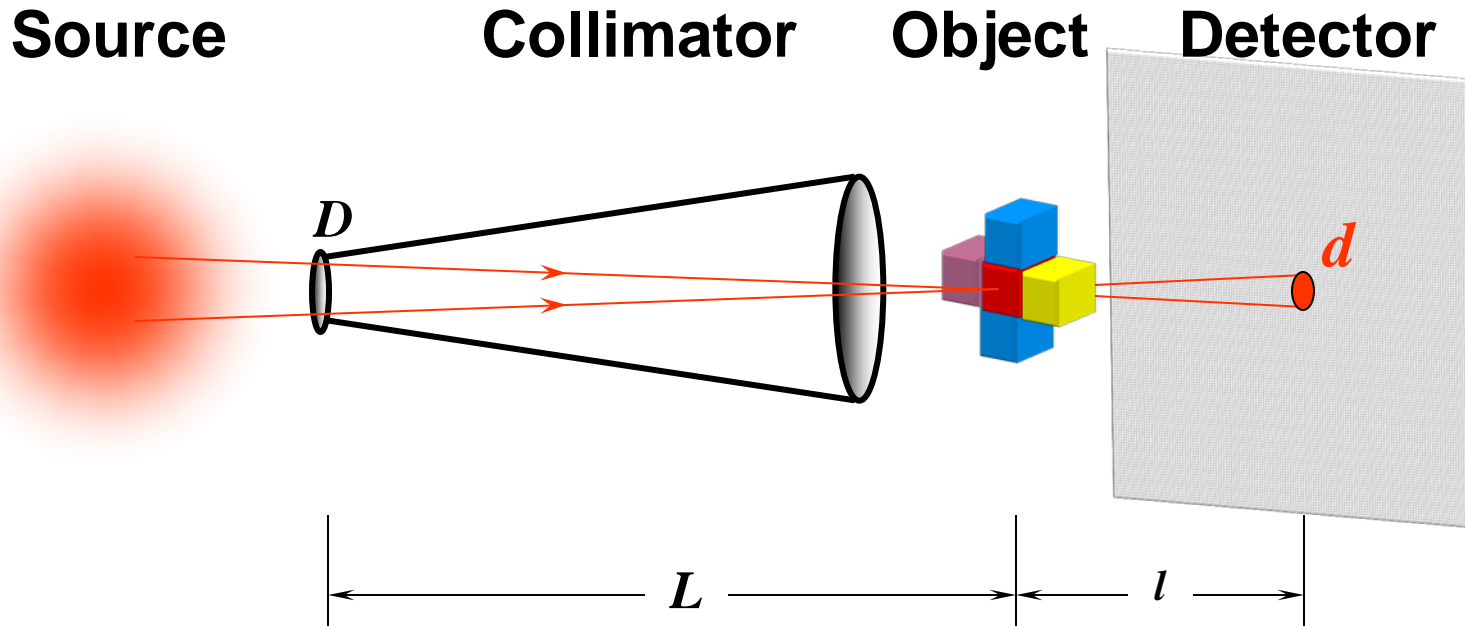
x – propagation direction

I_0 – primary beam

$\Sigma(x)$ – attenuation coefficient



Beam optimisation



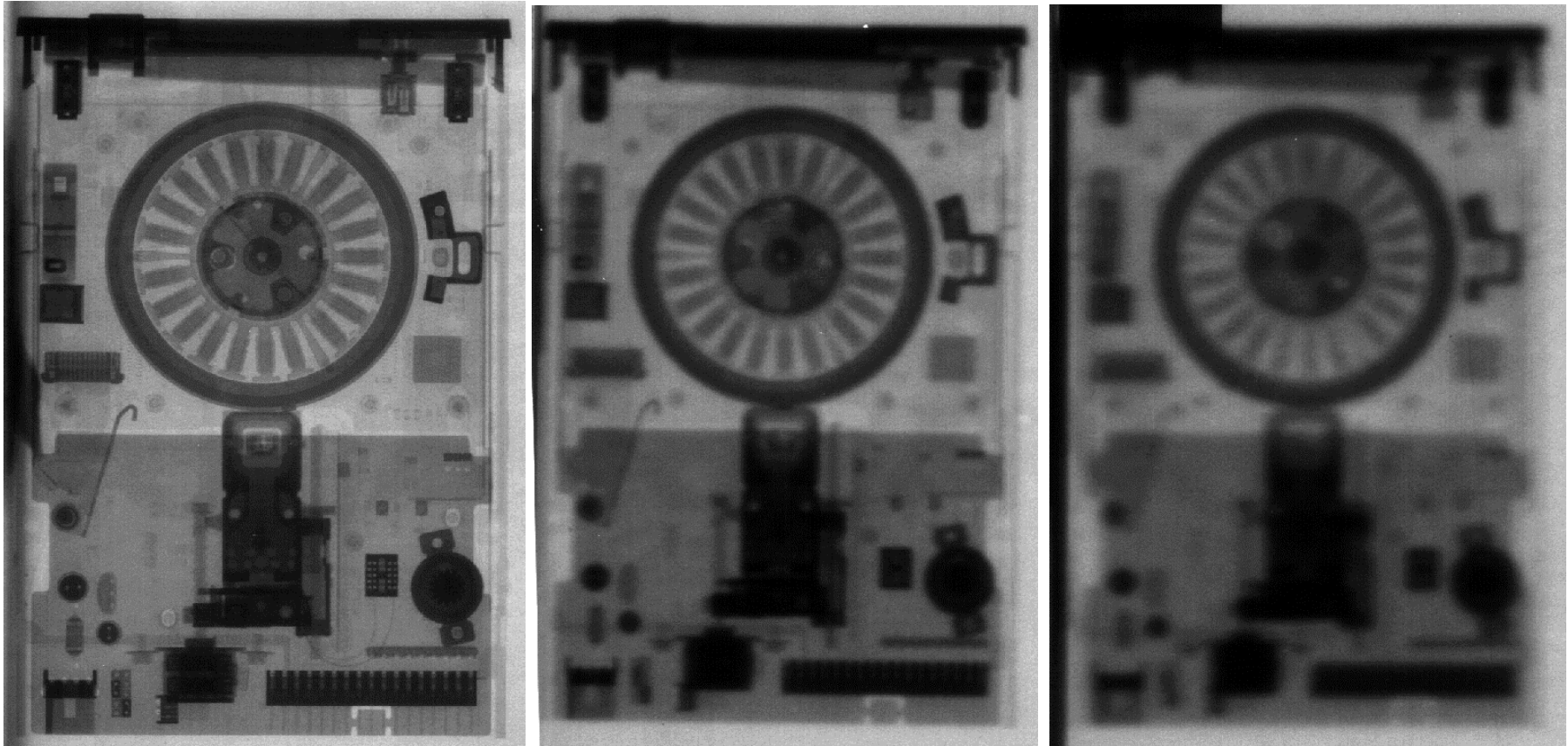
D – Collimator aperture

L – Distance Collimator-Object

l – Distance Object-Detector

$$d = \frac{l}{L/D}$$

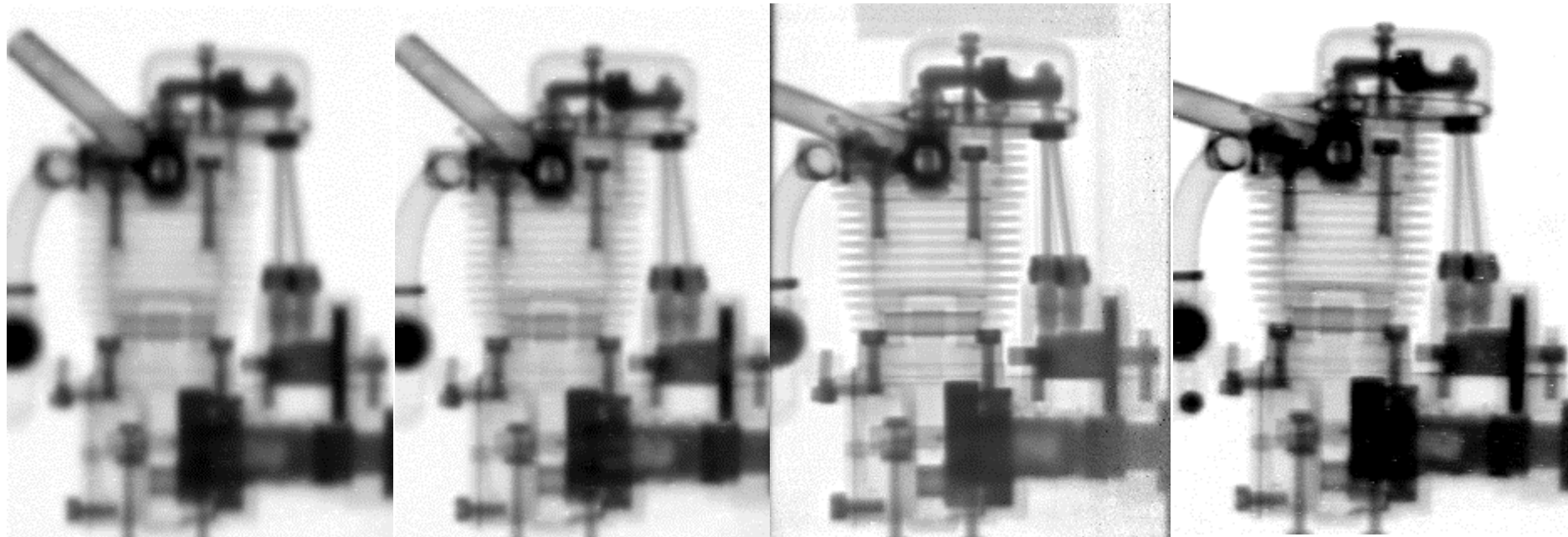
Beam optimisation



Radiographs of a 3,5" floppy drive in 0 cm, 10 cm and 20 cm distance from a film + Gd sandwich taken at a cold neutron guide with $L/D=71$.

B. Schillinger, Estimation and measurement of L/D on a cold and thermal neutron guide, in: Nondestructive Testing and Evaluation, World Conference on Neutron Radiography, vol. 16, Osaka, 1999, pp. 141–150

Beam optimisation



$L/D=71$

$L/D=115$

$L/D=320$

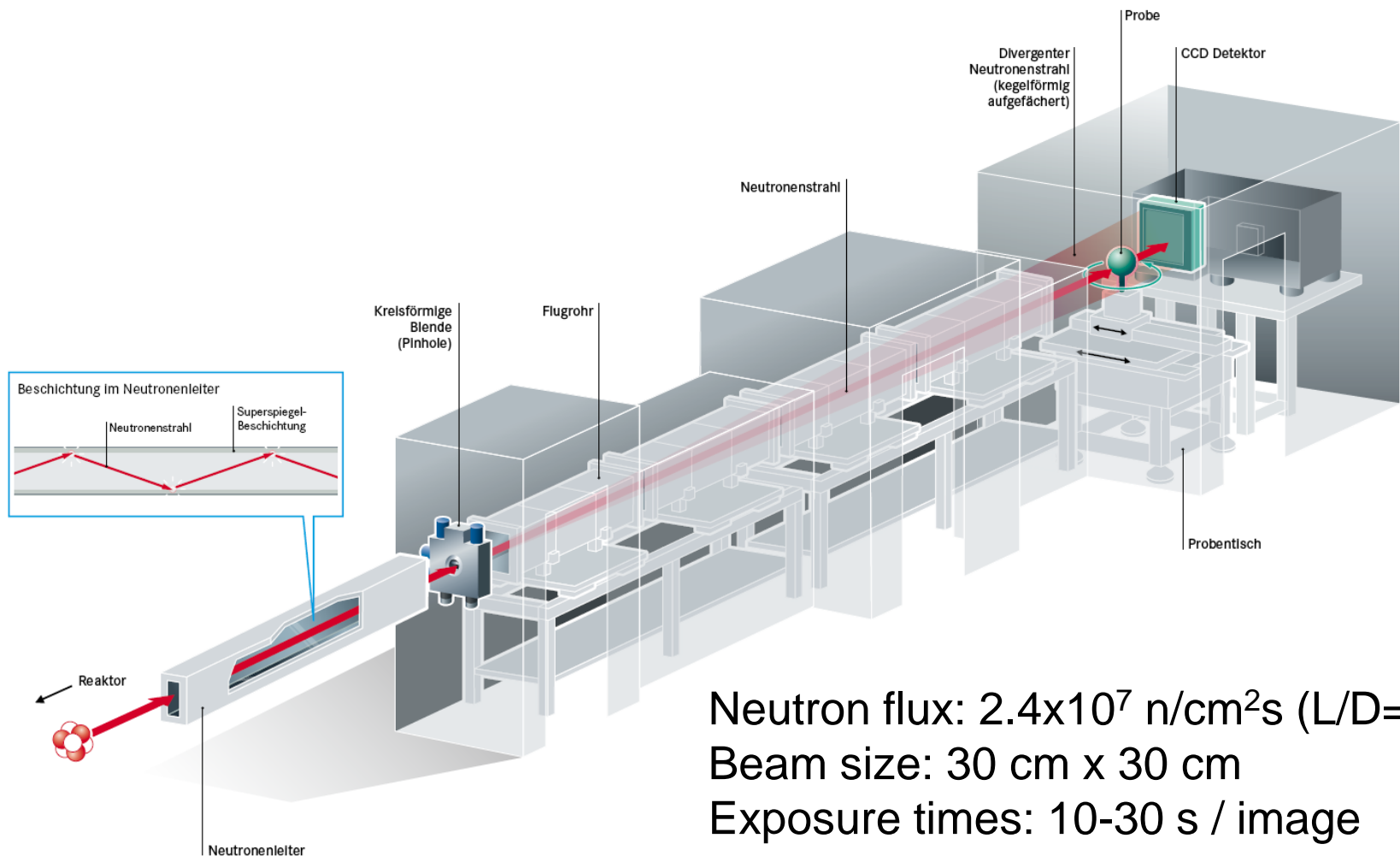
$L/D>500$.

Radiographs of a small motor taken at different beam positions
with different L/D ratios.

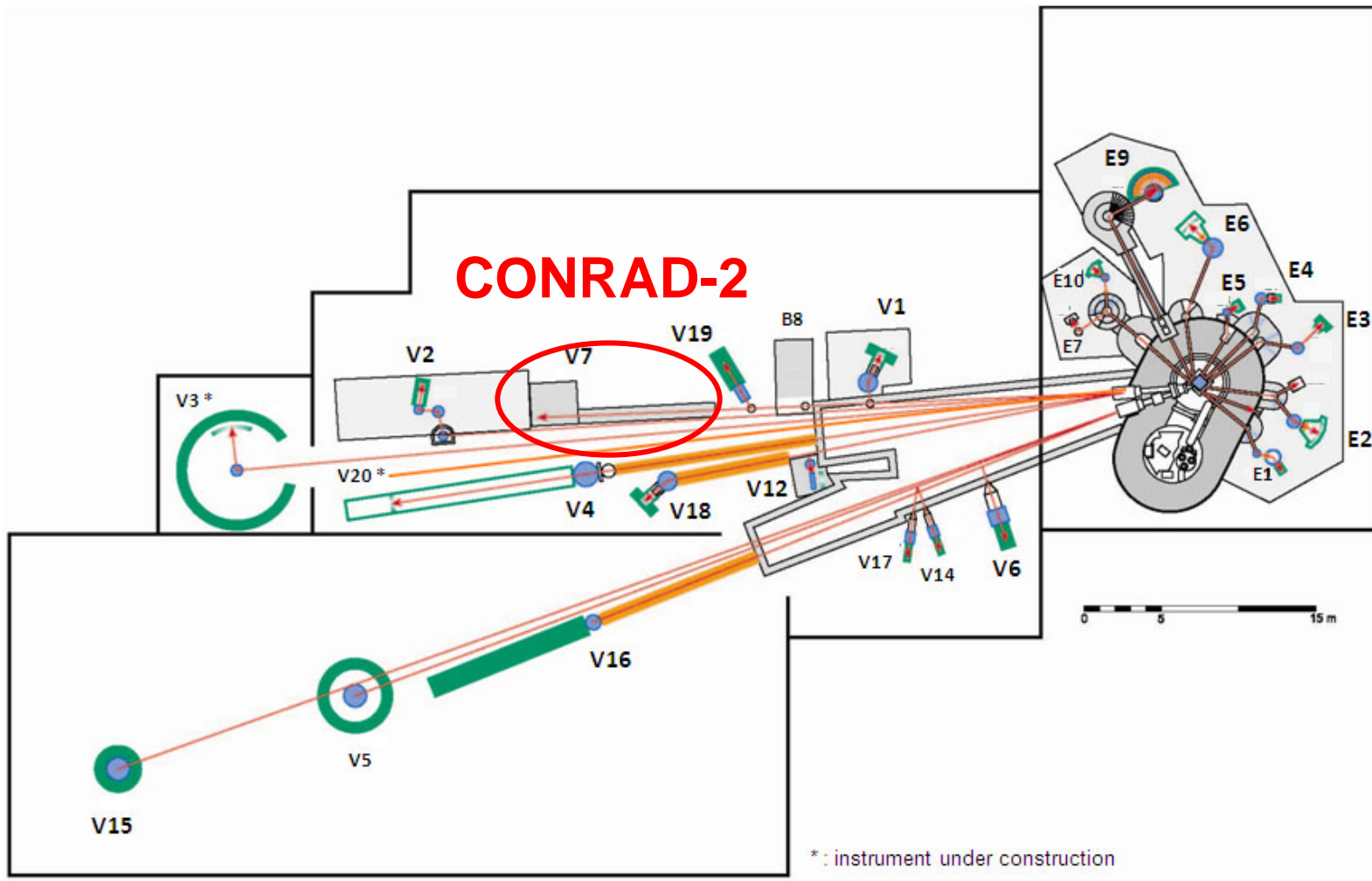
B. Schillinger, Estimation and measurement of L/D on a cold and thermal neutron guide, in: Nondestructive Testing and Evaluation, World Conference on Neutron Radiography, vol. 16, Osaka, 1999, pp. 141–150

Neutron imaging

CONRAD-2 Instrument



Beam optimisation







Resolution

- Beam optimisation
- Detector development 

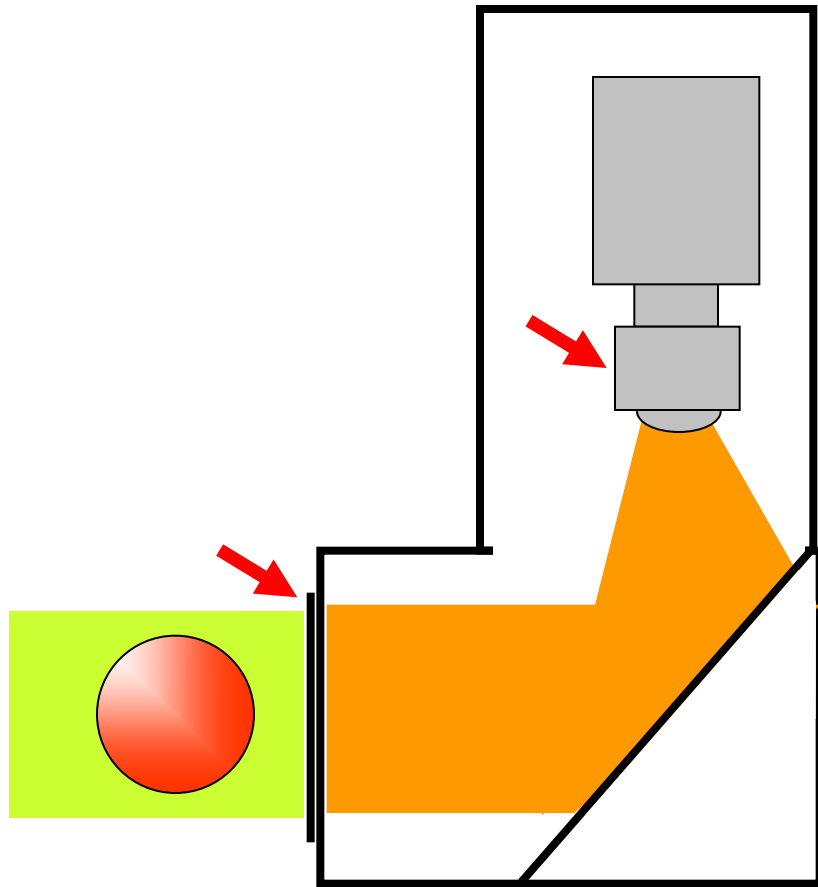
Contrast

- Neutron interaction with matter
 - absorption
 - scattering
 - magnetic interaction



Detector development

Detector system



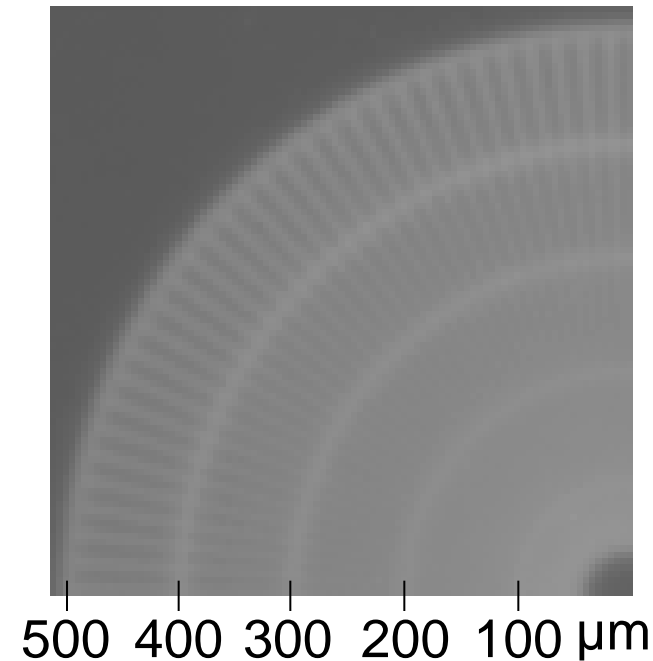
Standard setup

Scintillator: 200 µm 6LiF

Lens system: 50 mm

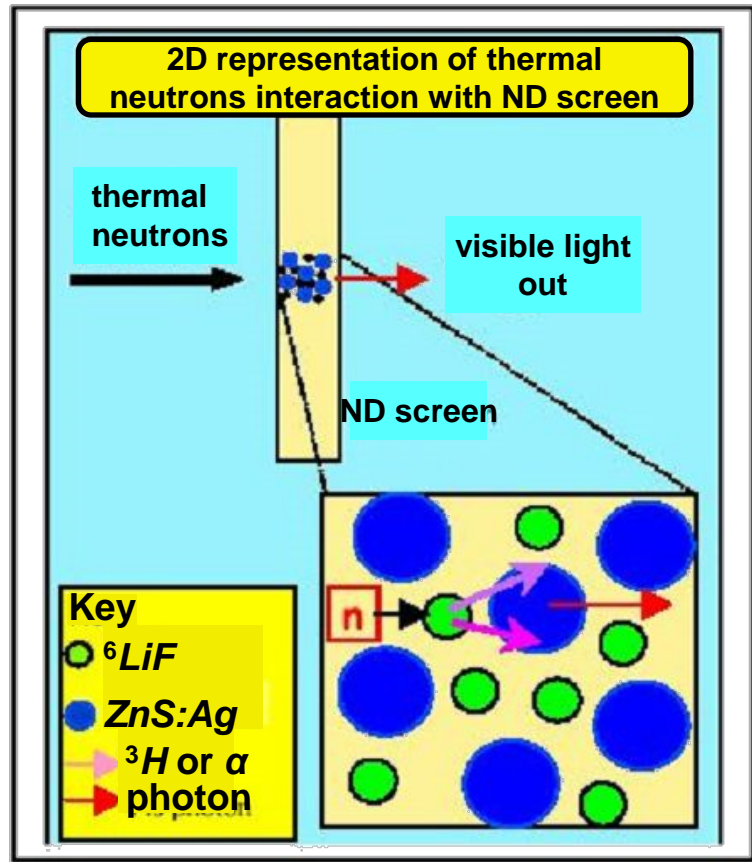
Pixel size: 100 µm

Exposure time: 20 s

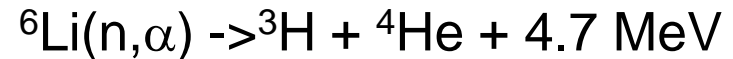


Detector development

The ZnS+⁶LiF scintillation screen is the limit of resolution.



The reaction products of



have to be stopped in the ZnS scintillation screen.

Their average range is in the order of 50-80 μm .

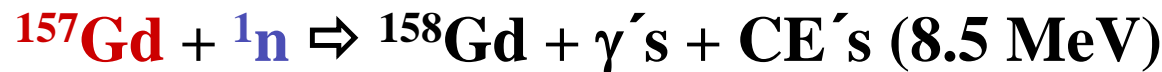
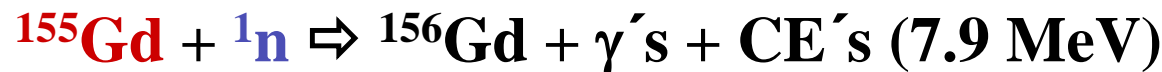
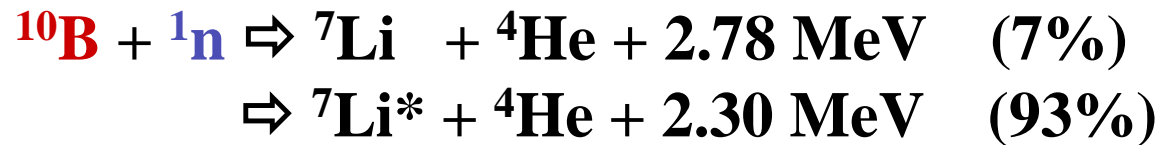
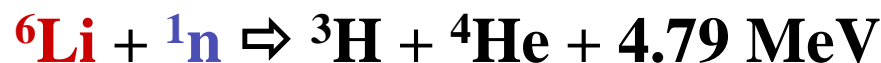
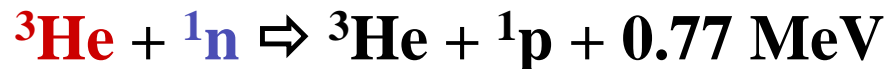
About 177,000 photons are generated per detected neutron.

With thinned scintillation screens, we can achieve resolution in the order of 20-30 μm .

Slide courtesy: Dr. Burkhard Schillinger (FRM-II, Munich, Germany)



Capture reactions for thermal / cold neutrons



Detector development

Nikkor Makro-Objektiv - 105 mm - F/2.8



FOV_{\max} : 10 cm x 10 cm, pixel size: 50 μm
 FOV_{\min} : 6 cm x 6 cm, pixel size: 30 μm

Nikon Micro Nikkor 200mm f/4 D (IF) ED



1:1 imaging
 FOV_{\max} : 2.8 cm x 2.8 cm, pixel size: 13.5 μm



Detector development

Detector development

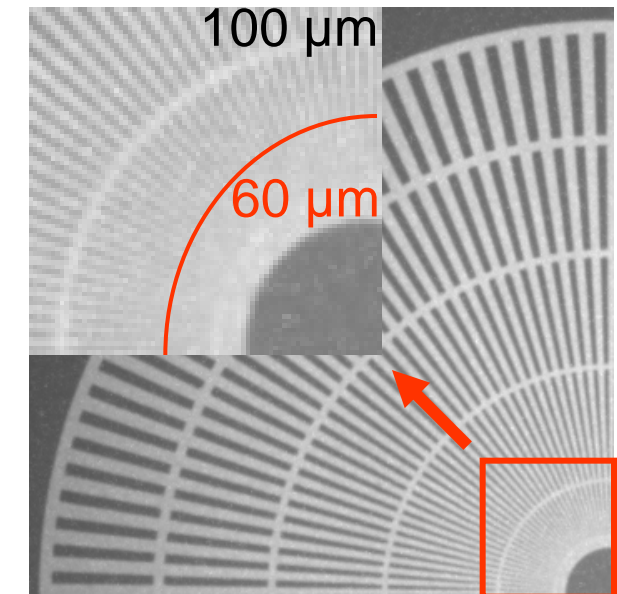
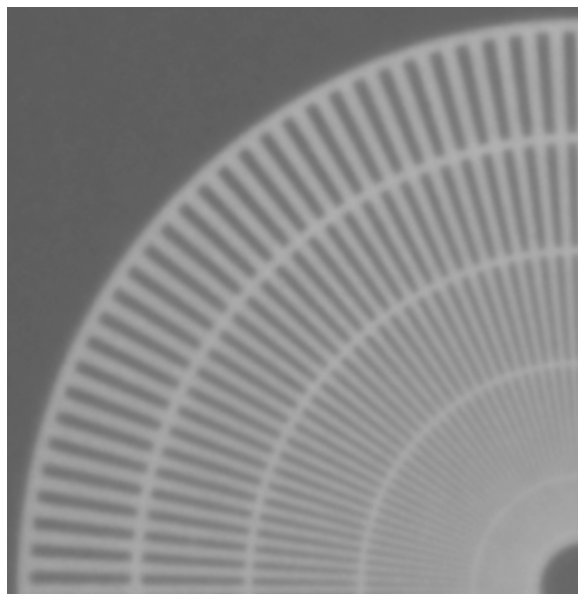
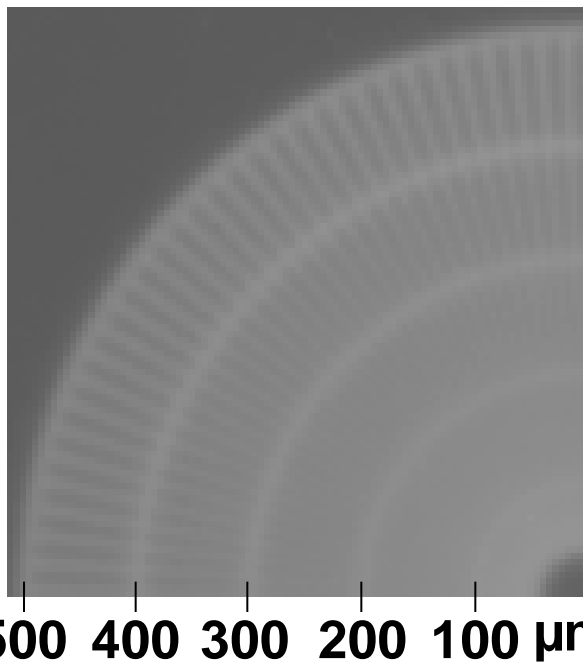
Standard setup

Improved lenses+ Improved screen

Scintillator: 200 μm 6LiF
Pixel size: 100 μm
Exposure time: 20 s

Scintillator: 200 μm 6LiF
Pixel size: 30 μm
Exposure time: 20 s

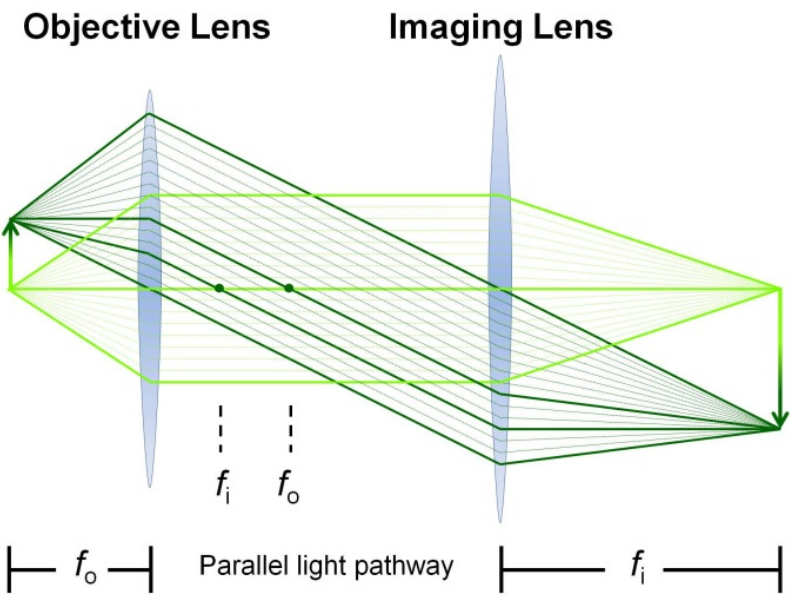
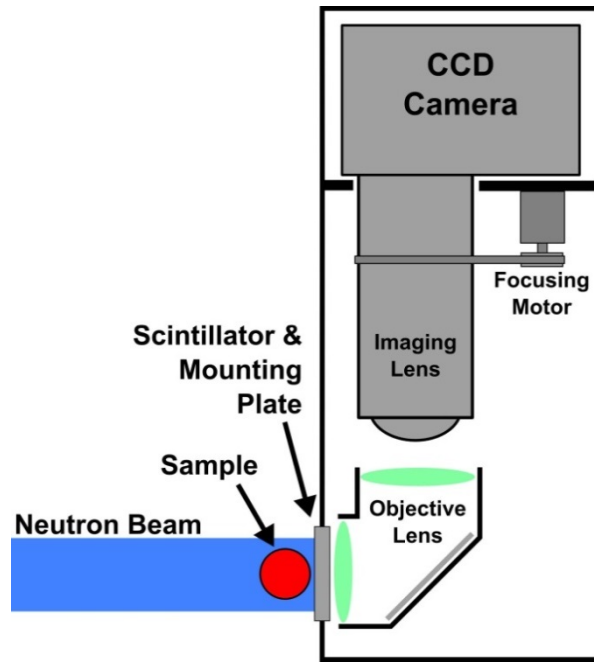
Scintillator: 5 μm Gadox
Pixel size: 30 μm
Exposure time: 120 s



Kardjilov, N., et al. "A highly adaptive detector system for high resolution neutron imaging." *Nuclear Instruments and Methods in Physics Research Section A: Accelerators, Spectrometers, Detectors and Associated Equipment* 651.1 (2011): 95-99.



High resolution

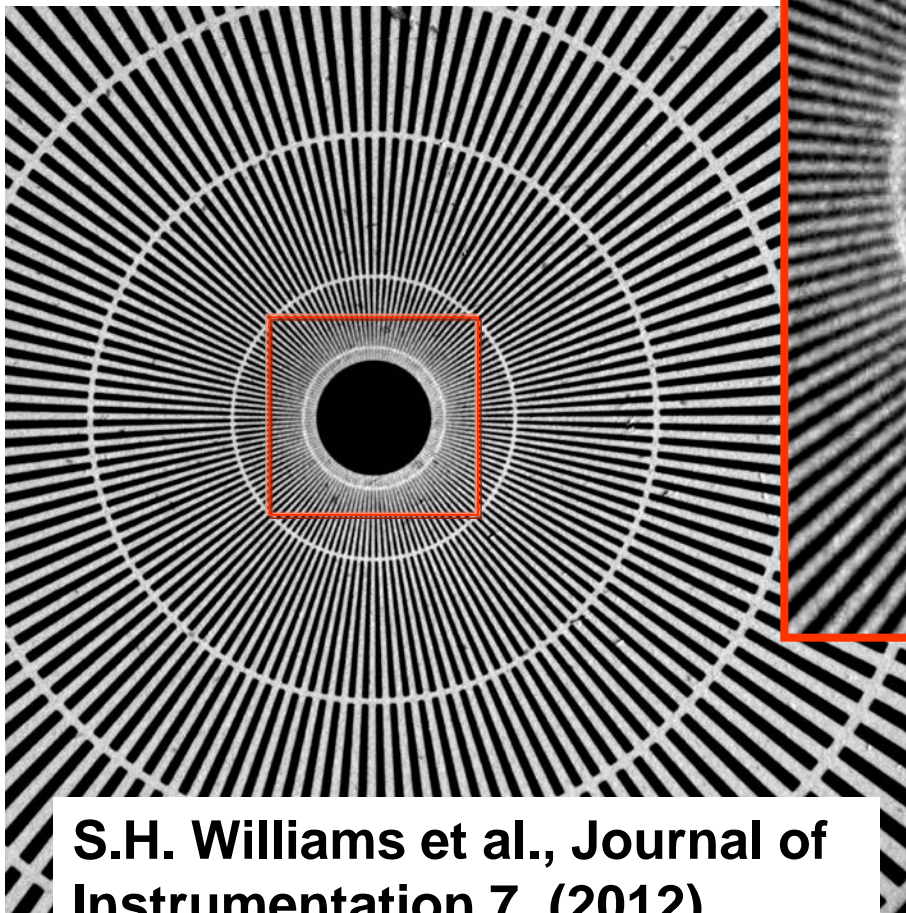


<i>Obj. Lens/Img. Lens</i>	<i>M</i>	<i>P_{eff}</i> (μm)	<i>FOV</i> (mm)
105 mm / 50 mm	2.10	6.429	13.2×13.2
200 mm / 100 mm	2.00	6.750	13.8×13.8
200 mm / 50 mm	4.00	3.375	6.9×6.9

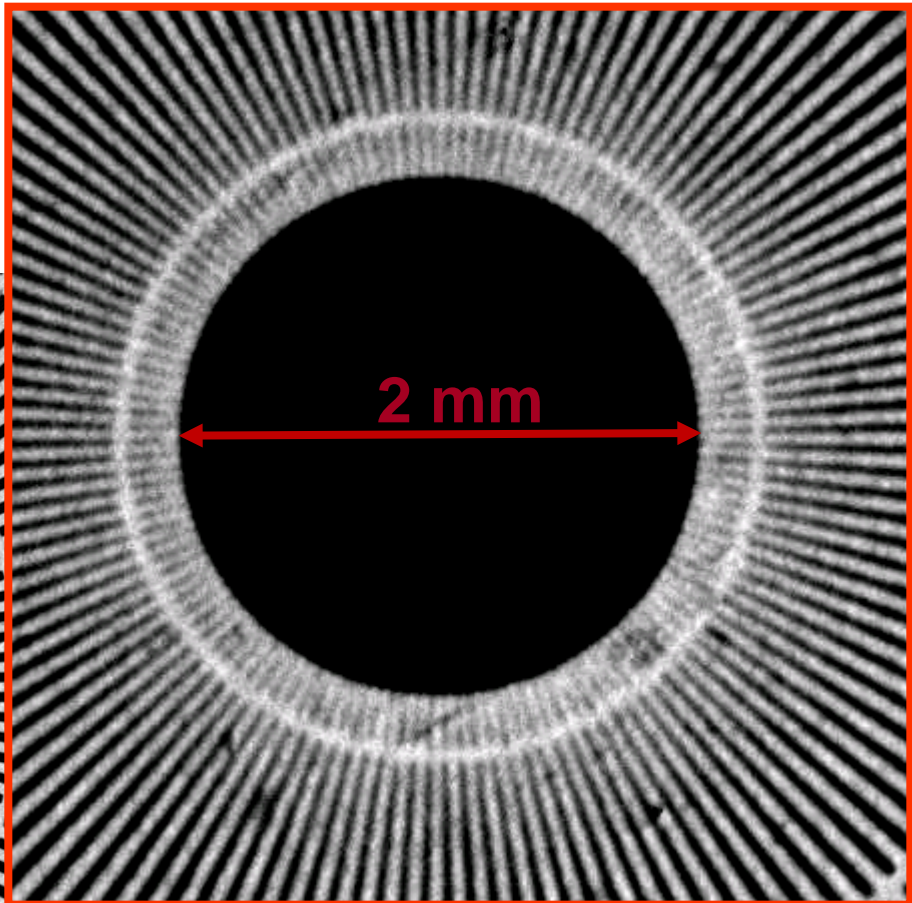
S. H. Williams et al, J. of Instrumentation (2012)



Adaptive high-resolution imaging



S.H. Williams et al., Journal of
Instrumentation 7, (2012)



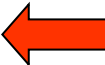
Camera: Andor DW436
Lens system: Magnification
Pixel size = 3.375 μm
Szintillator: GGG
Resolution: 7.9 μm (63.2 lp/mm)



Resolution

- Beam optimisation
- Detector development

Contrast

- Neutron interaction with matter
 - absorption 
 - scattering
 - magnetic interaction 



- absorption



- scattering

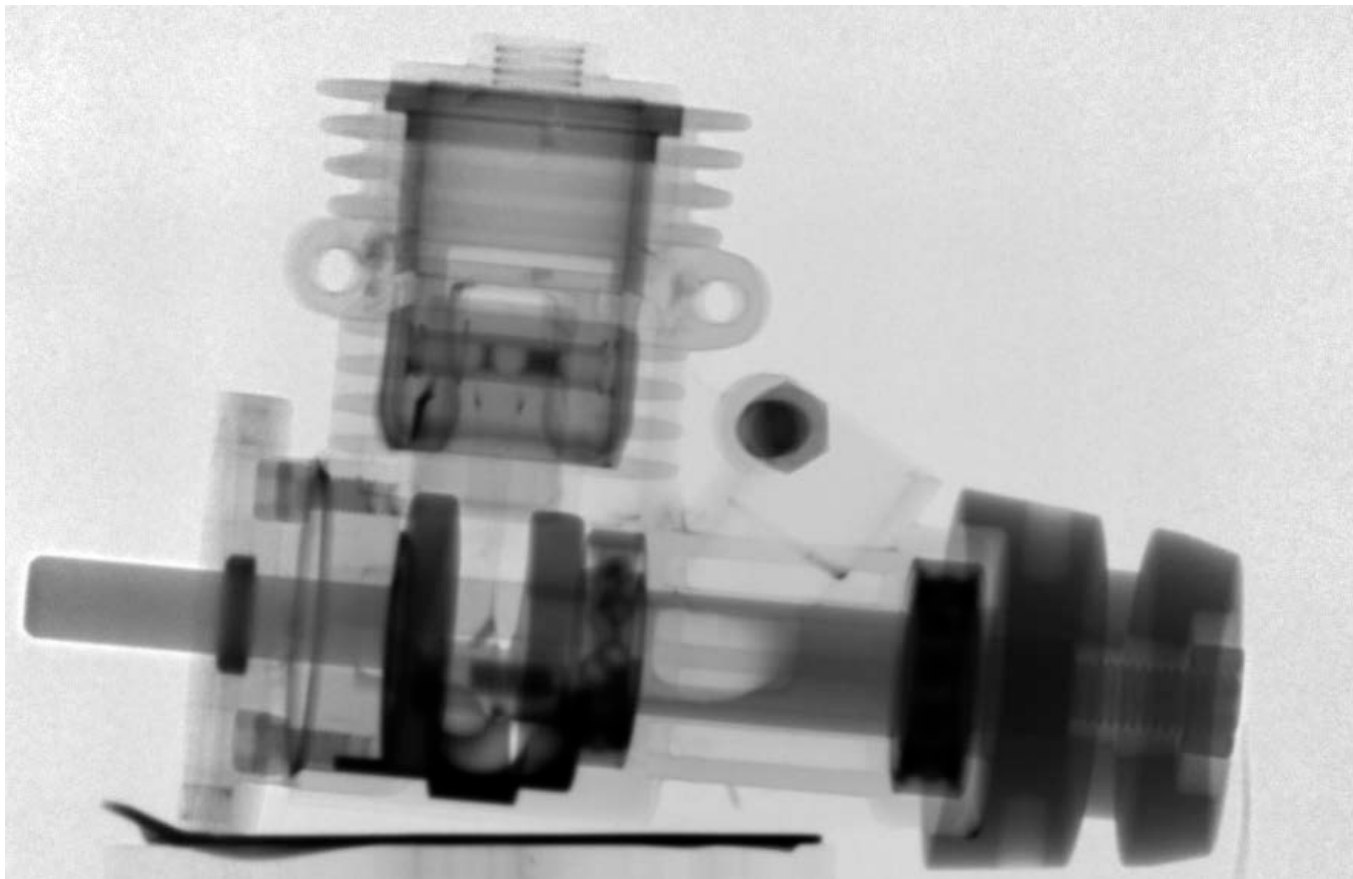


- magnetic interaction



Attenuation Contrast

n

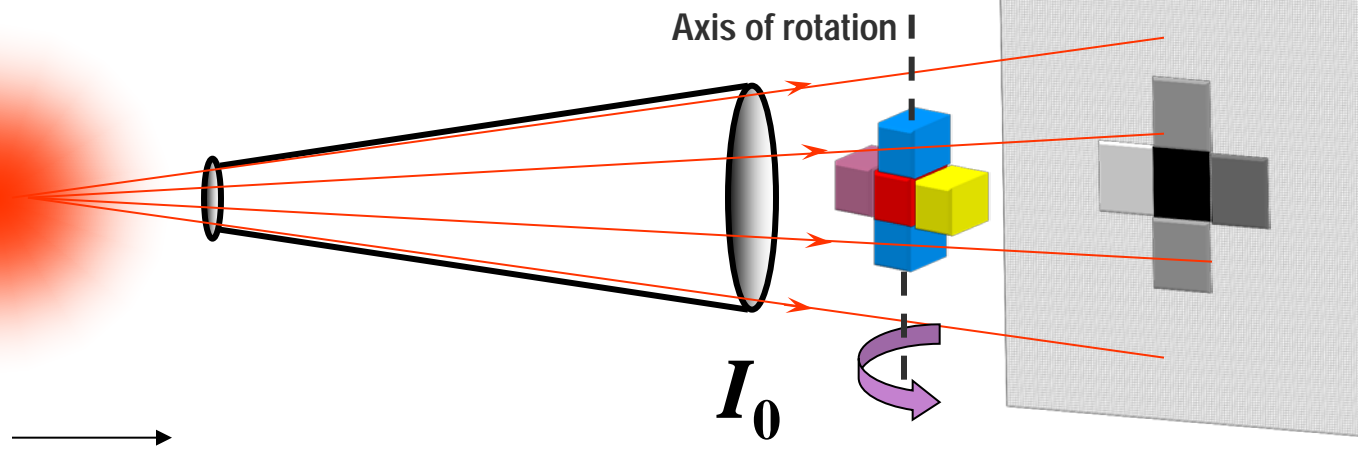


1 cm

Attenuation Contrast

Absorption tomography

Source Collimator Object Detector



I_0

Tomography

$$\sim I_0 e^{-\int \Sigma(x) dx}$$

x – propagation direction

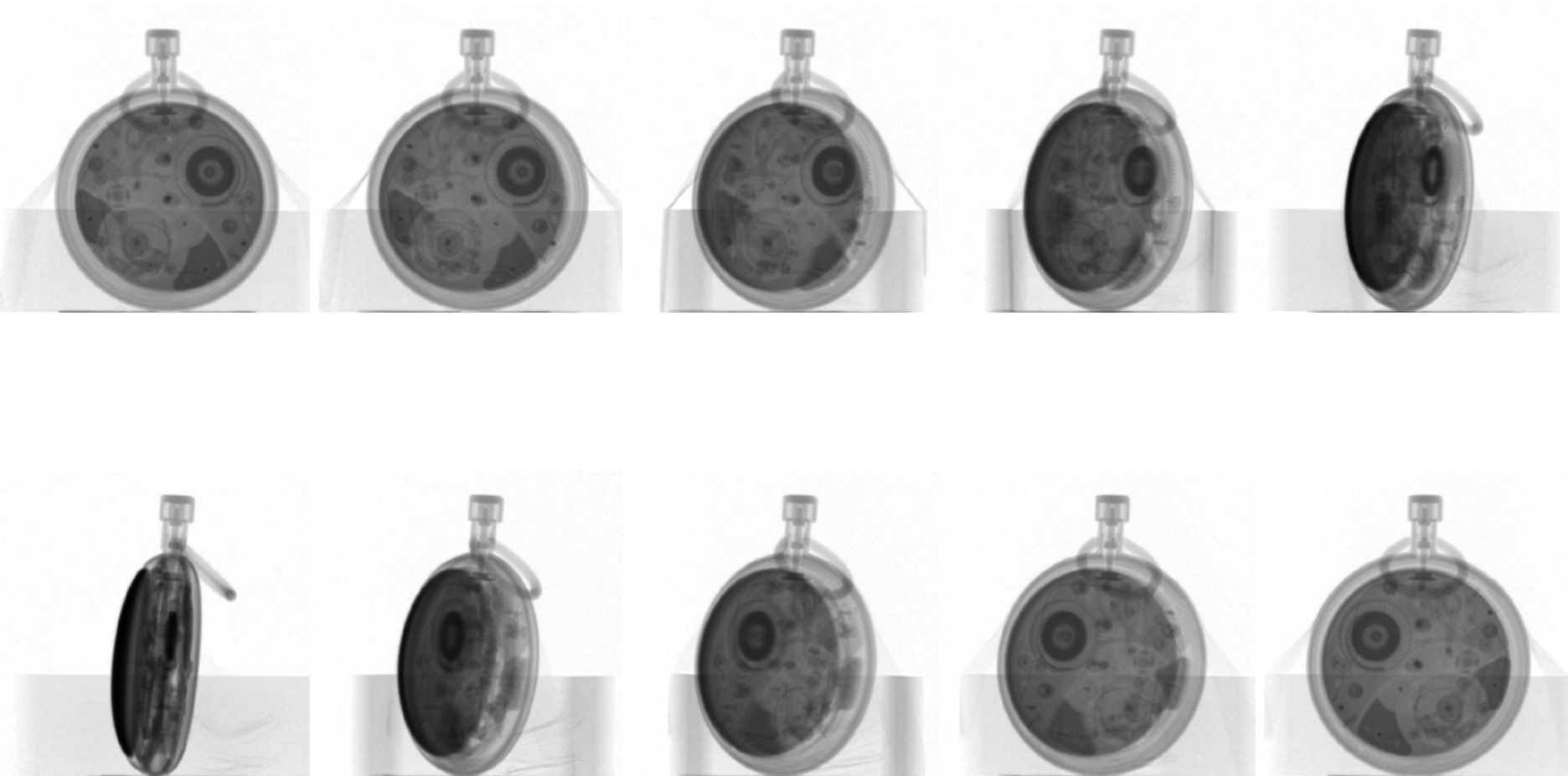
I_0 – primary beam

$\Sigma(x)$ – attenuation coefficient



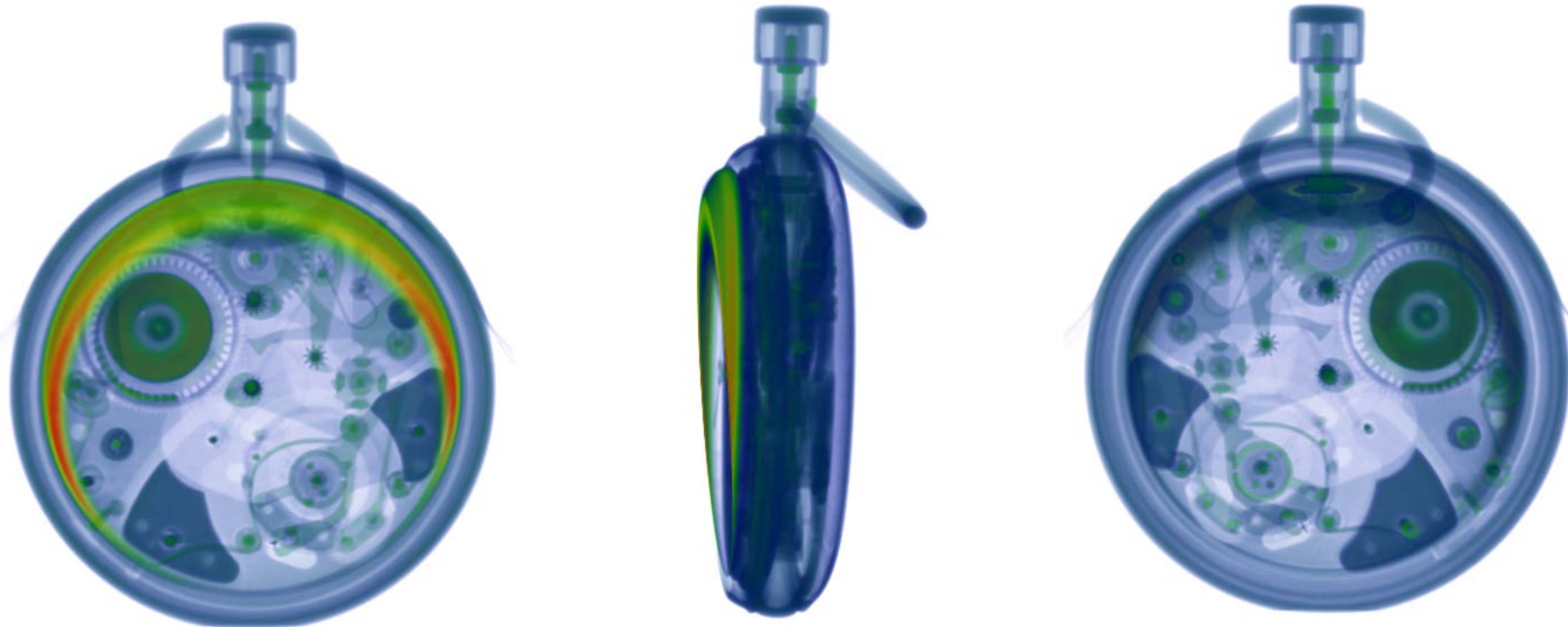
Neutron imaging

Single tomographic projections

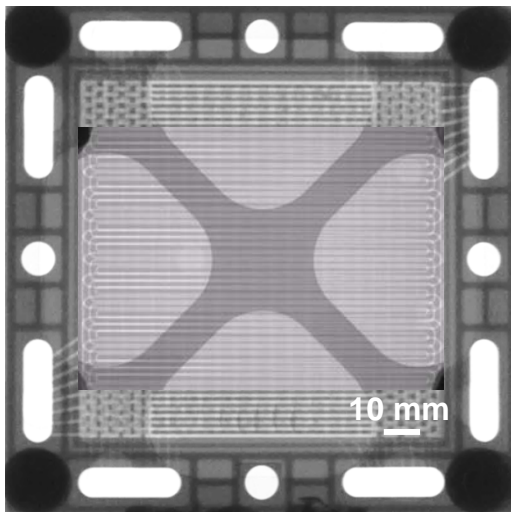


Neutron imaging

Tomographic reconstruction



How to optimize water management in a PEM fuel cell?



- *In-operando visualization of water distribution*

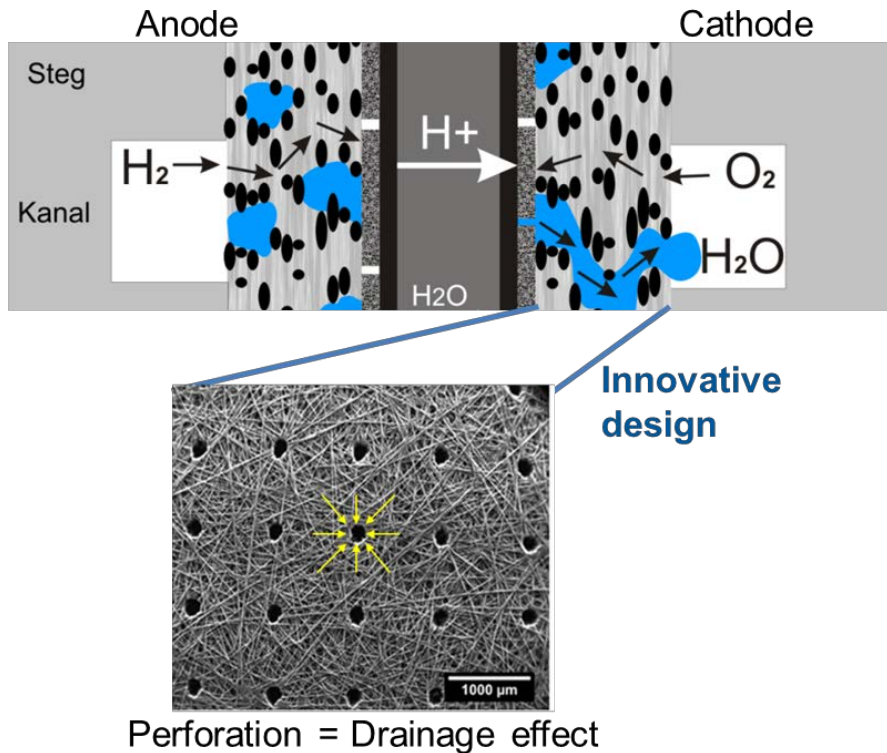
Diffusion dynamics revealed with D-H contrast



Photons: tailor-made microporosity improves water transport

- Optimized electrode design
- Improved performance under varying operation conditions

How to optimize water management in a PEM fuel cell?



- *In-operando visualization of water distribution*

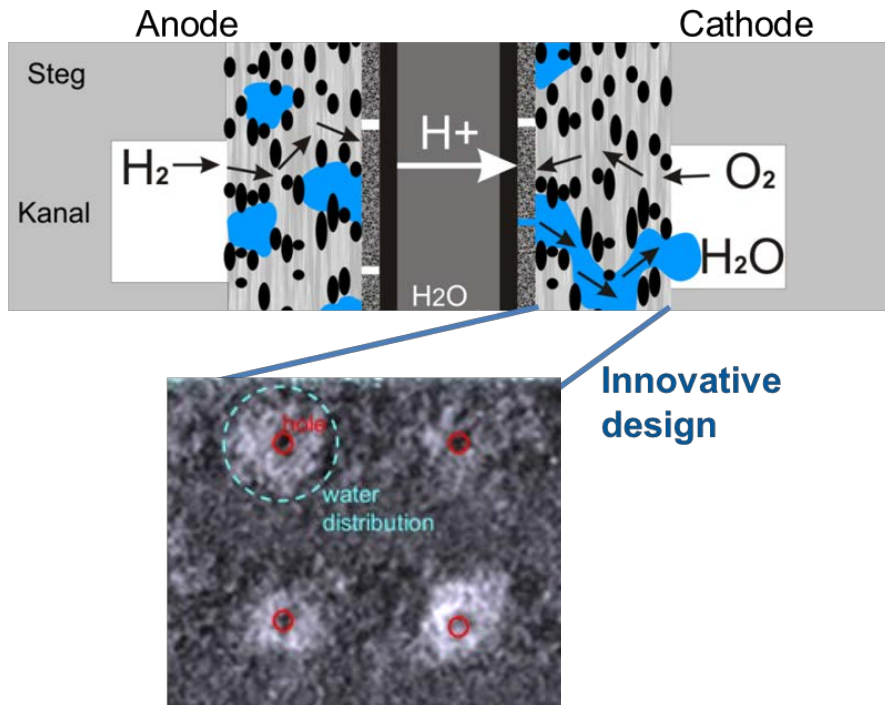
Diffusion dynamics revealed with D-H contrast

Photons: tailor-made microporosity improves water transport

→ Optimized electrode design

→ Improved performance under varying operation conditions

How to optimize water management in a PEM fuel cell?



Neutron tomography slice
(pixel size: 6.5 μm , 600 projections /360°, time: 8 h)

- *In-operando visualization of water distribution*

Diffusion dynamics revealed with D-H contrast

Photons: tailor-made microporosity improves water transport

J. Haußmann *et al.*, Journal of Power Sources 239 (2013) 611

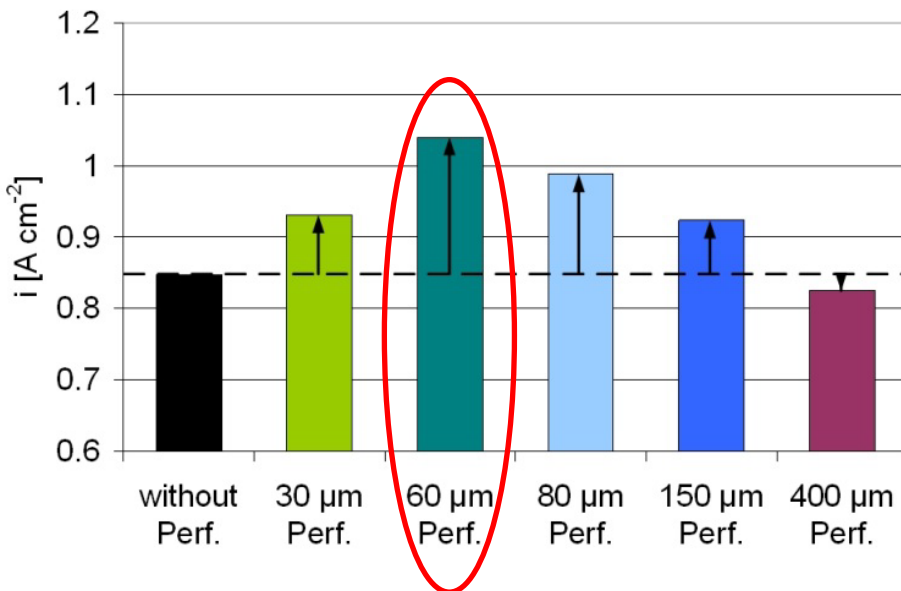
→ Optimized electrode design

→ Improved performance under varying operation conditions

How to optimize water management in a PEM fuel cell?

Best case: 40% performance increase

Typical: 10-20% increase



- *In-operando* visualization of water distribution

Diffusion dynamics revealed with D-H contrast

Photons: tailor-made microporosity improves water transport

Material now in production

→ Optimized electrode design

→ Improved performance under varying operation conditions



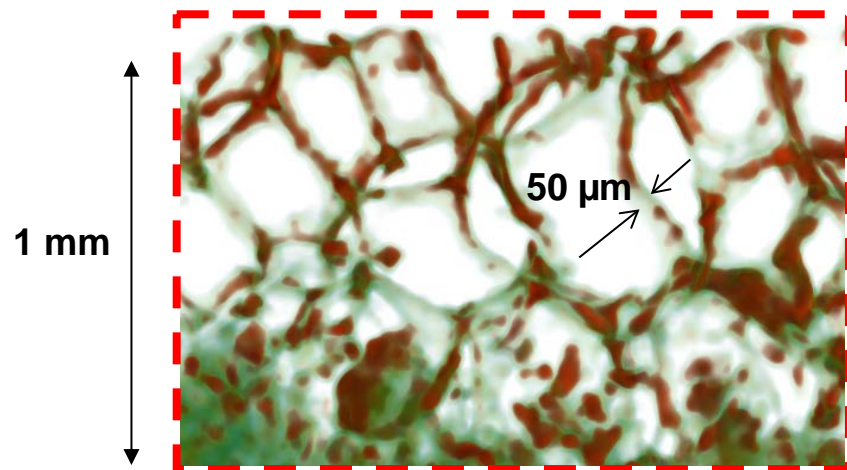
ELECTROLYSER ELECTRODES

A. Tengattini
N. Lenoir
D. Atkins

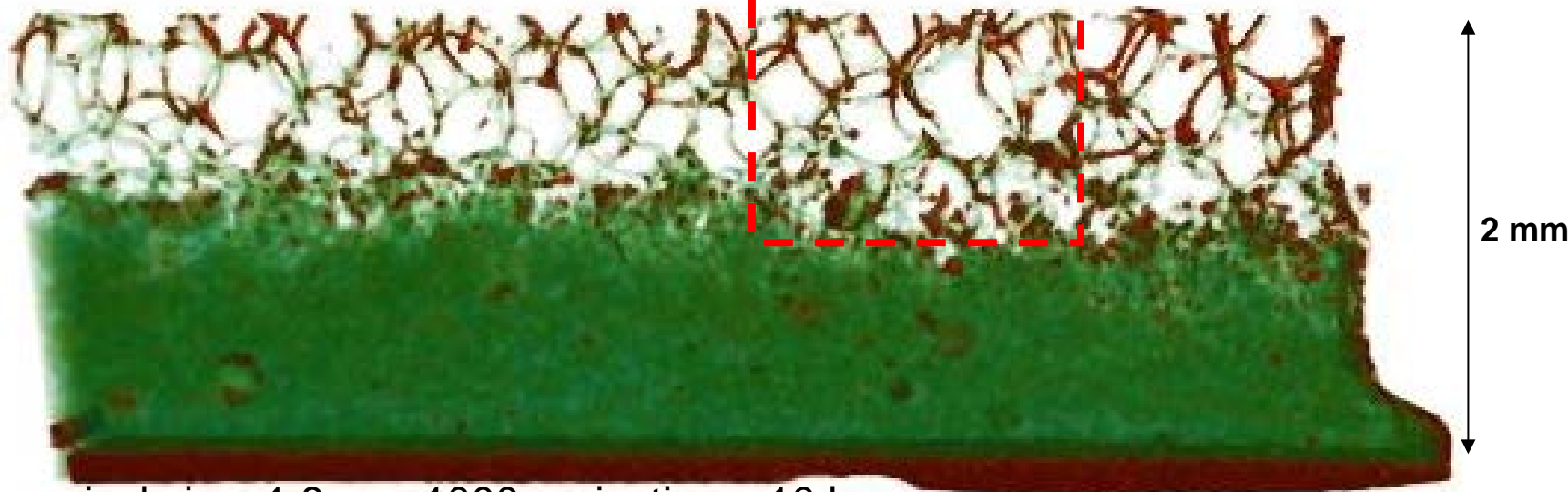


Ni mesh
polymer coating

↔
2 mm

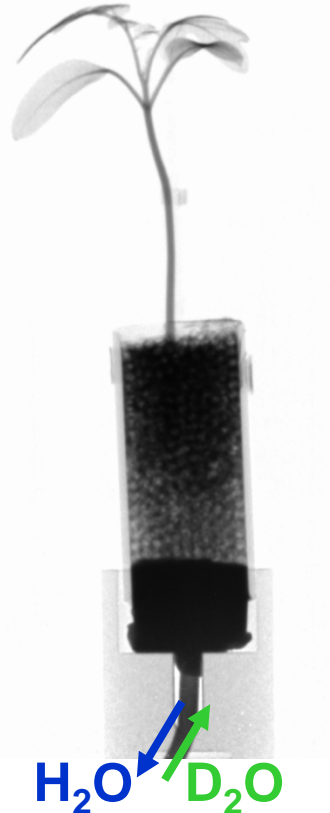


High-resolution tomography @ ILL (D50)



pixel size: 1.8 μm , 1000 projections, 10 hours

How to observe the water uptake in plant's root



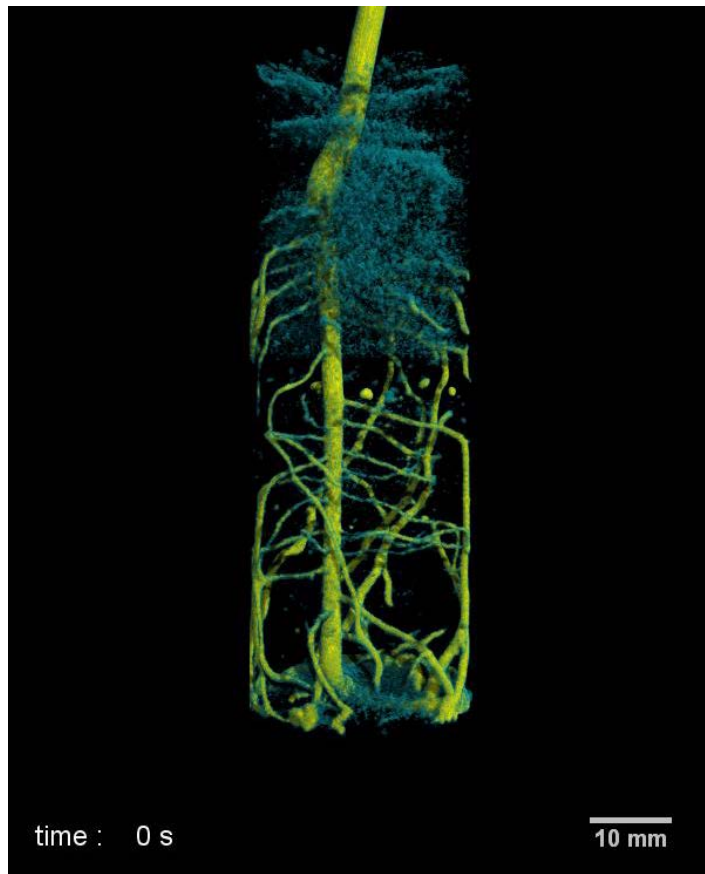
- *In-operando 3D visualization of water distribution*

Water uptake dynamics revealed with D-H contrast

Insights in the water uptake mechanisms in the root system

- Observation of the dynamic processes in root system
- Learning about the root-soil interaction mechanisms

How to observe the water uptake in plant's root



High-speed (on-the-fly) neutron tomography

resolution: 150 µm

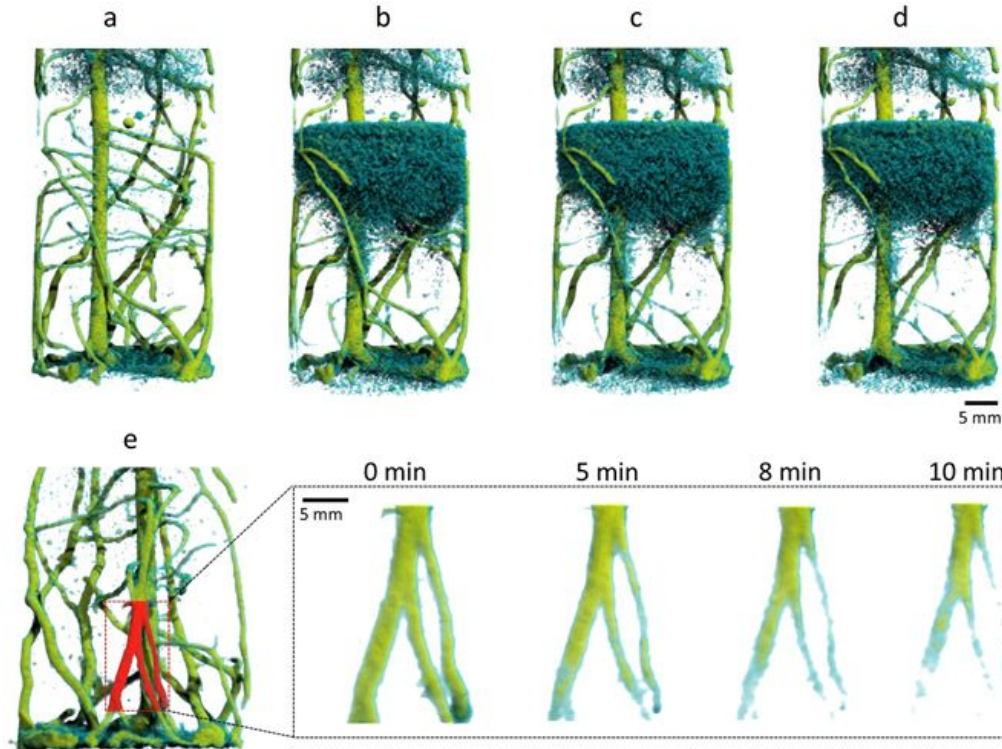
exposure: 0.05 s

200 projections/180°

10 s / tomography

- Observation of the dynamic processes in root system
- Learning about the root-soil interaction mechanisms

How to observe the water uptake in plant's root



High-speed (on-the-fly) neutron tomography

resolution: 150 µm

exposure: 0.05 s

200 projections/180°

10 s / tomography

Time series of neutron tomograms at (a) 0 min; (b) 5 min; (c) 8 min and (d) 10 min after feeding D₂O.

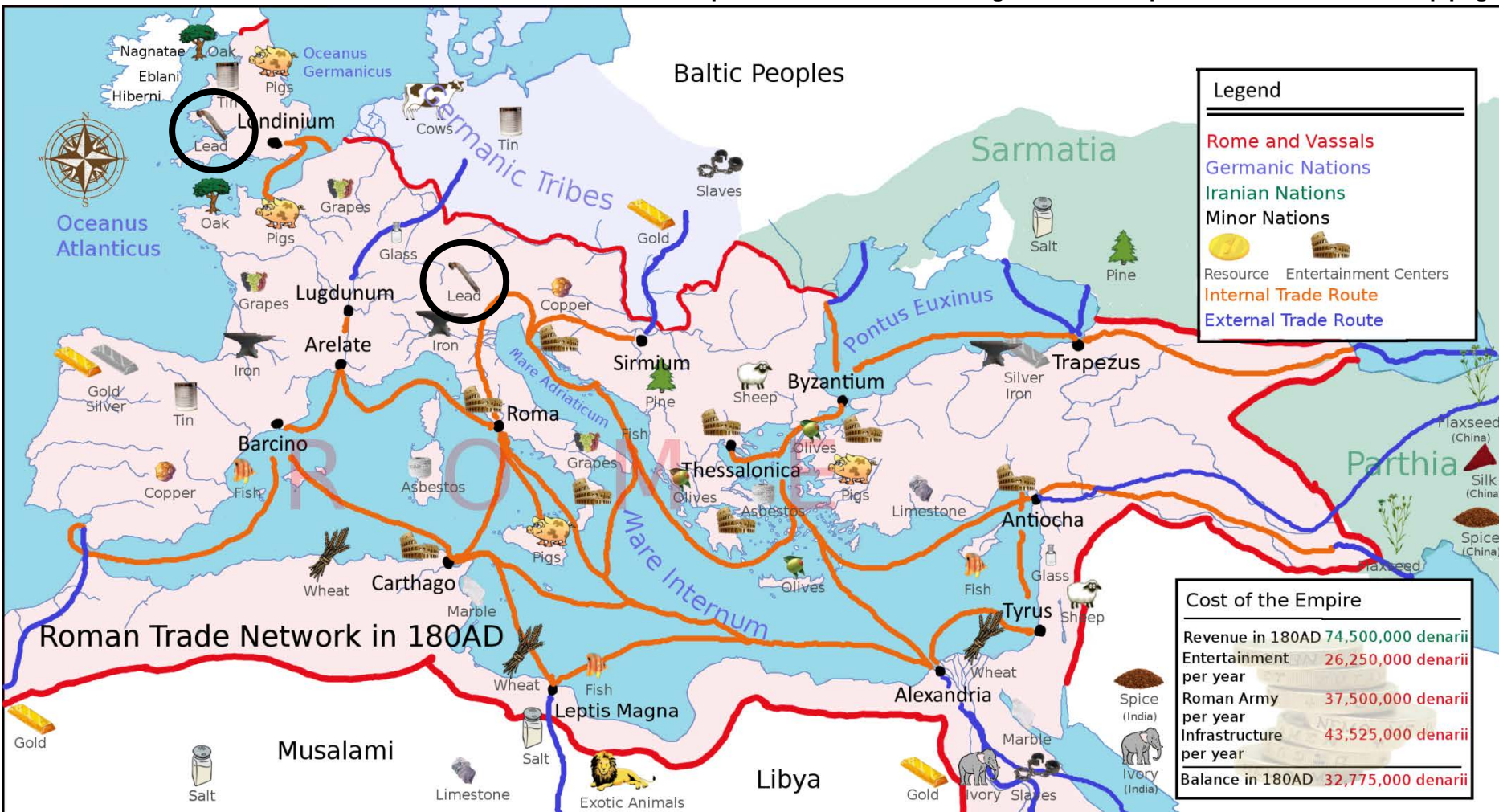
Ch. Tötzke, et al. *Scientific reports* 7.1 (2017): 6192.

- Observation of the dynamic processes in root system
- Learning about the root-soil interaction mechanisms

Attenuation Contrast

Shipwrecks

https://commons.wikimedia.org/wiki/File:Europe_180ad_roman_trade_map.png

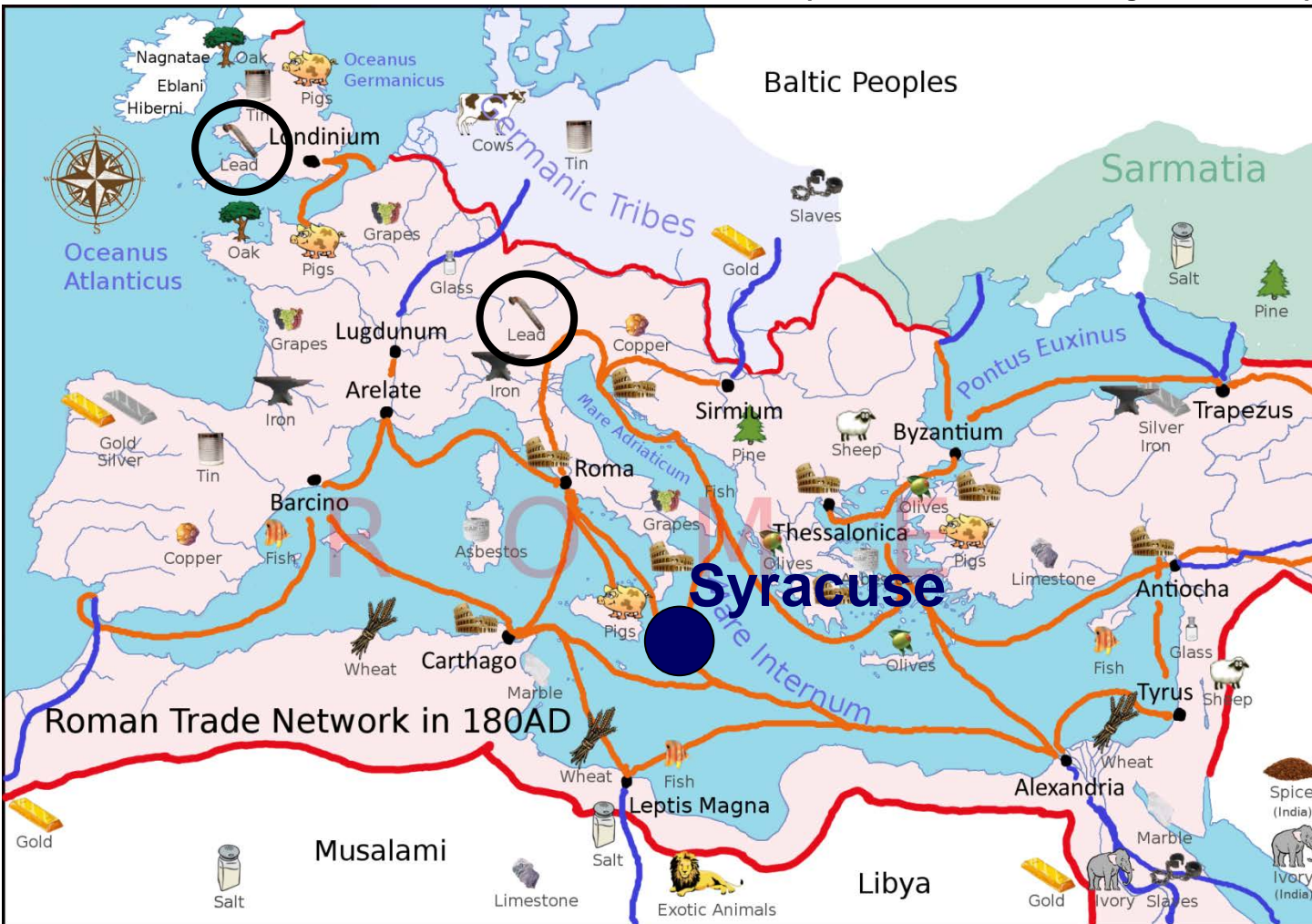


All routes lead to Rome: A map of Roman ports and trade routes

Attenuation Contrast

Shipwrecks

https://commons.wikimedia.org/wiki/File:Europe_180ad_roman_trade_map.png

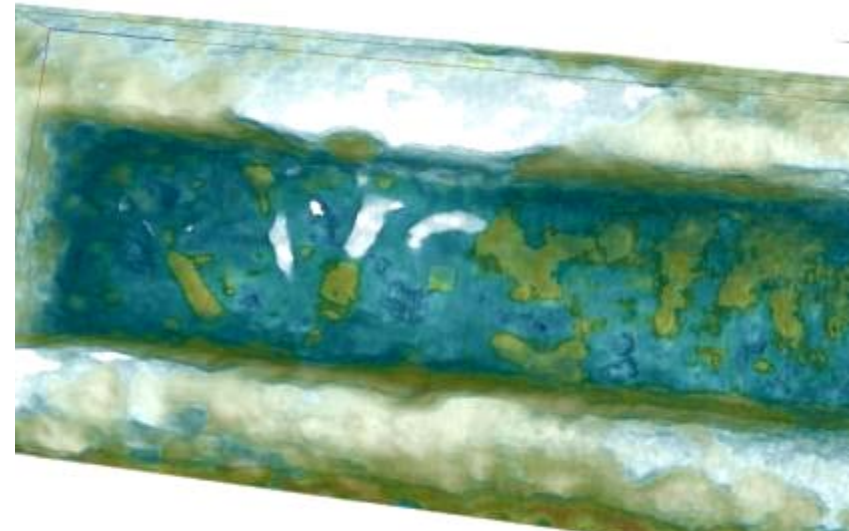
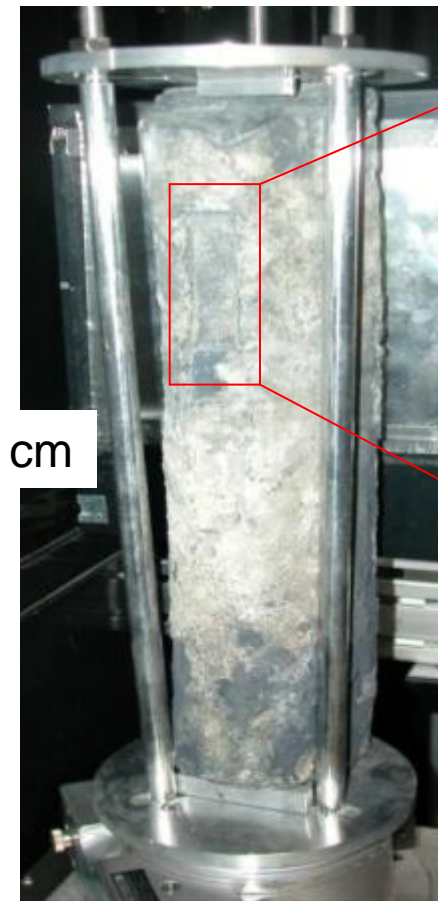


All routes lead to Rome: A map of Roman ports and trade routes



Attenuation Contrast

Lead blocks recovered near the UNESCO World Heritage Site Syracuse.
Presumably I century B.C. (Roman Imperial Age).

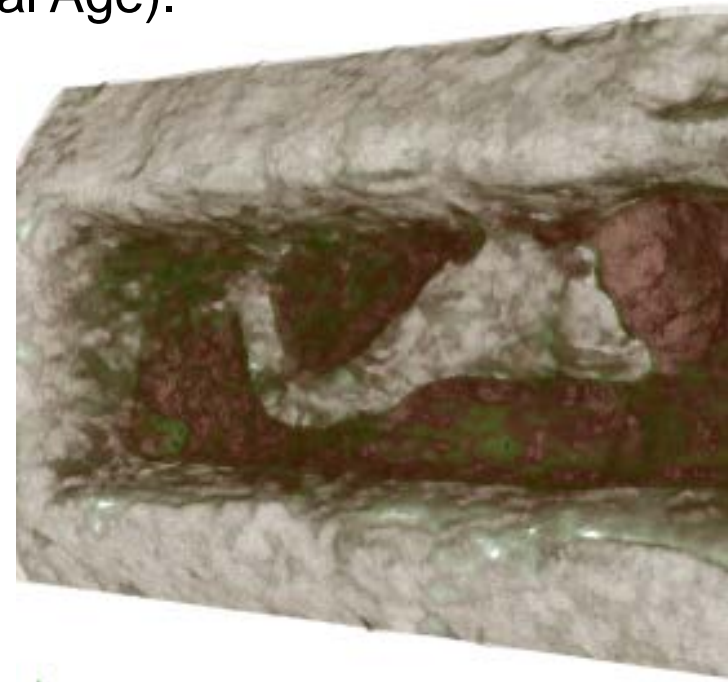
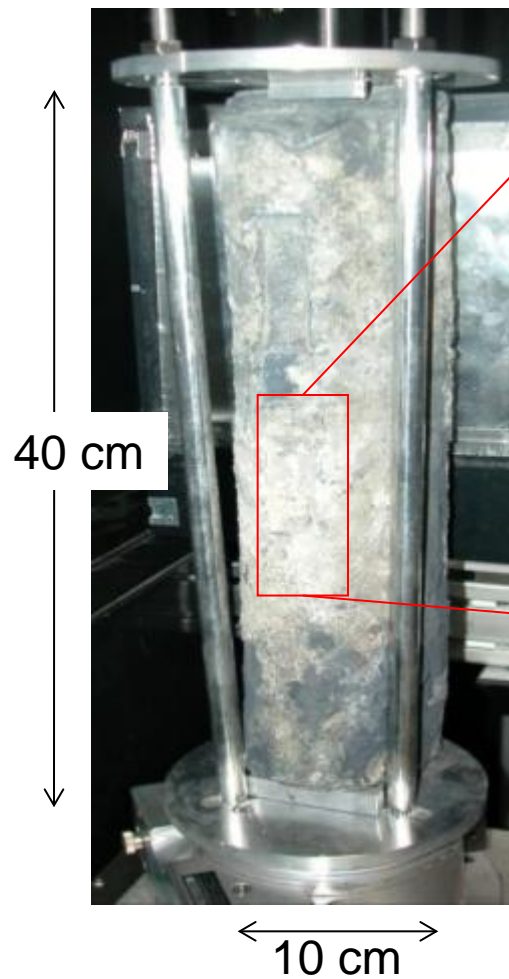


Triolo, R. et al, Neutron tomography of ancient lead artefacts, Anal. Methods 6 (2014) 2390-2394



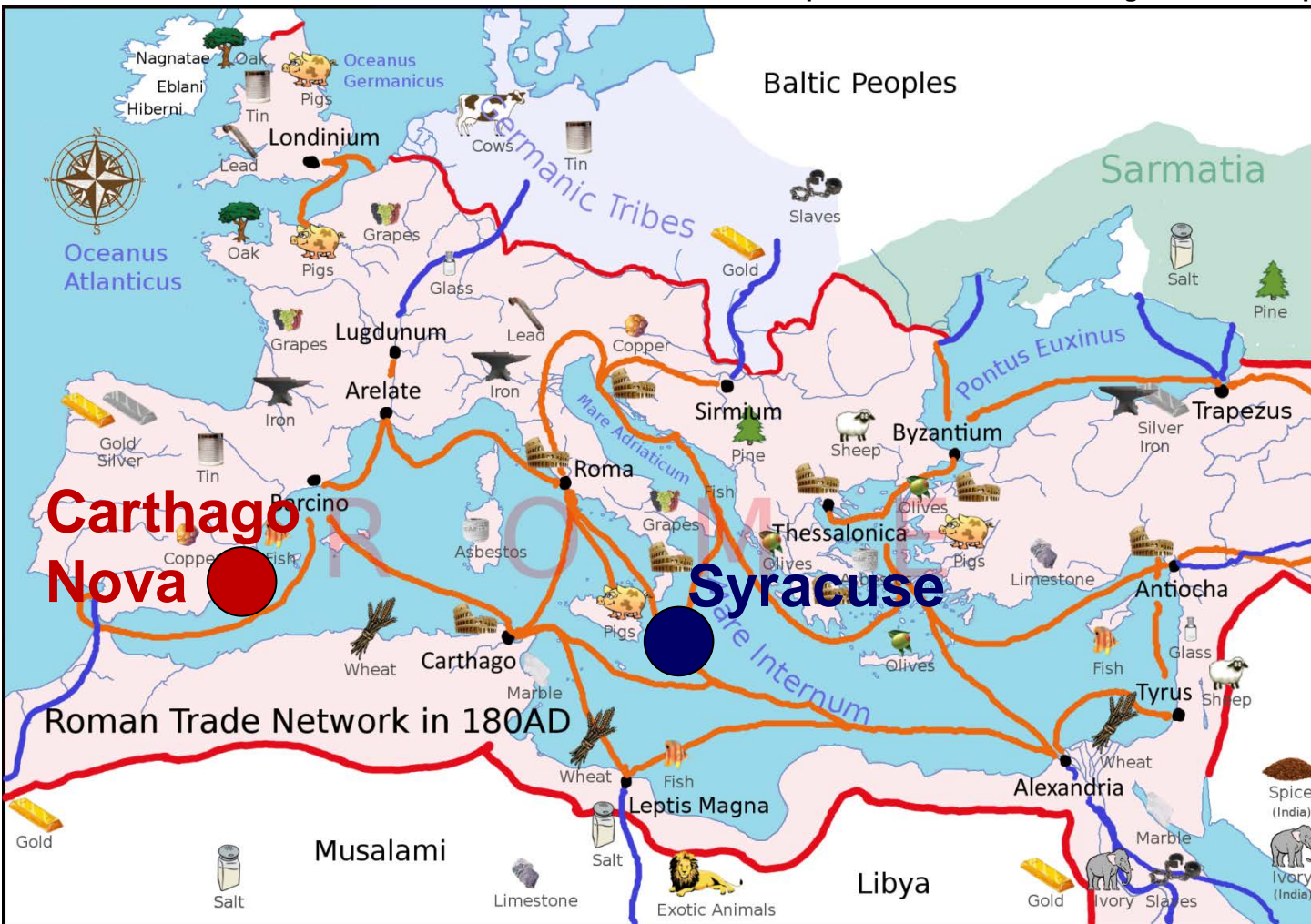
Attenuation Contrast

Lead blocks recovered near the UNESCO World Heritage Site Syracuse.
Presumably I century B.C. (Roman Imperial Age).



Attenuation Contrast

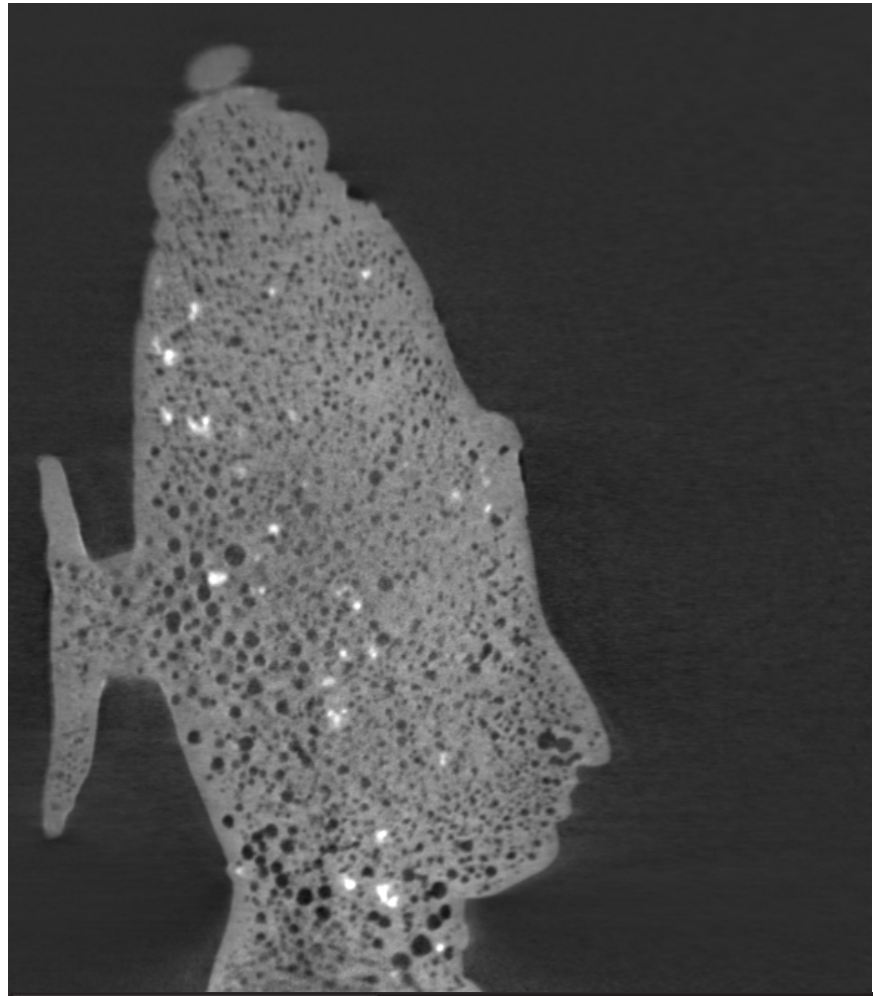
https://commons.wikimedia.org/wiki/File:Europe_180ad_roman_trade_map.png



Triolo, R., et al. *Analytical Methods* 6.7 (2014): 2390-2394.

N. Kardjilov, Oxford School on Neutron Scattering, 11. September 2019

Neutron tomography of bronze statues



RIJKS MUSEUM
a m s t e r d a m



Resolution

- Beam optimisation
- Detector development

Contrast

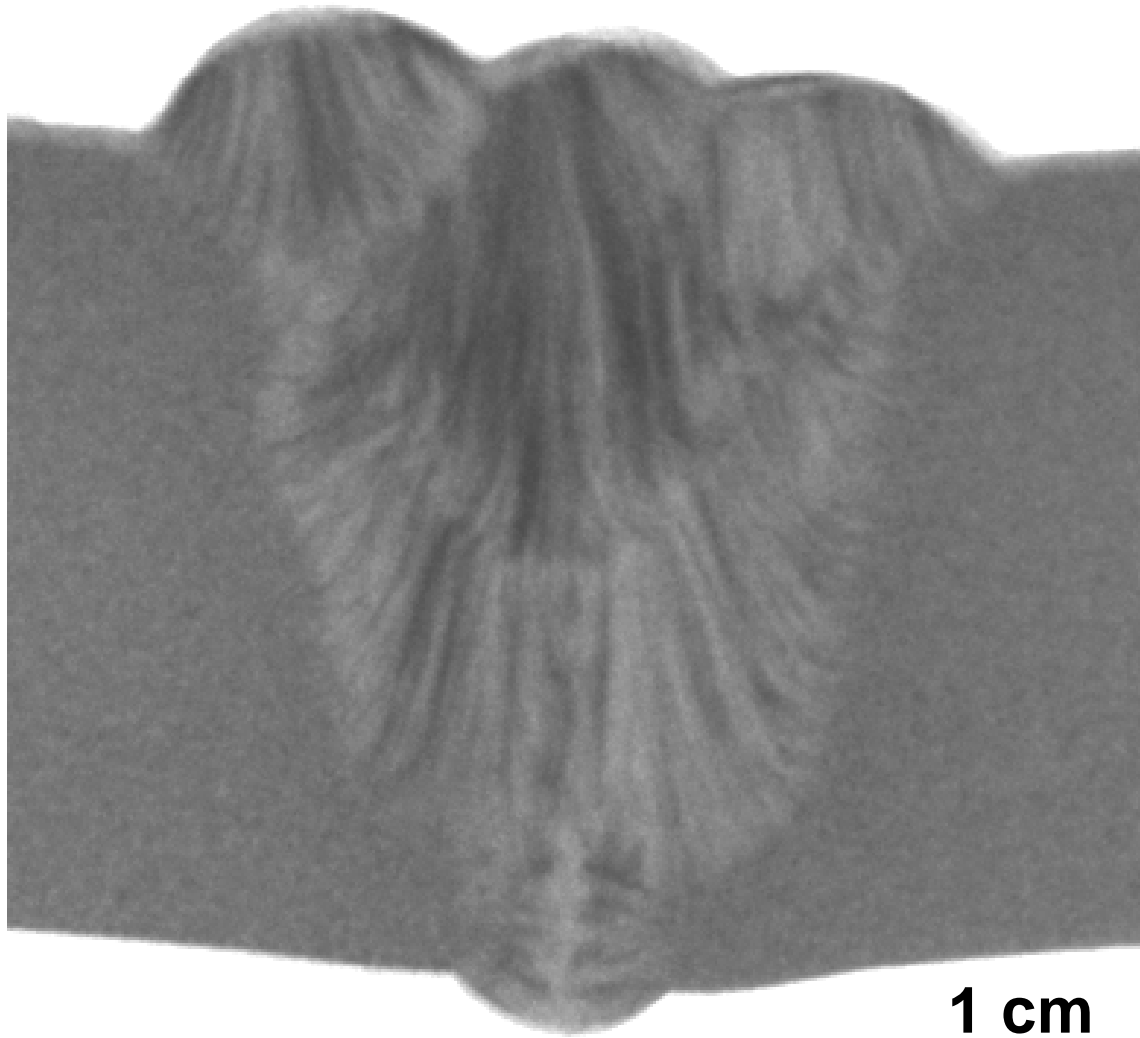
- Neutron interaction with matter
 - absorption
 - scattering 
 - magnetic interaction





Diffraction Contrast

$\lambda = 4.0 \text{ \AA}$





Diffraction Contrast

Beam monochromatisation

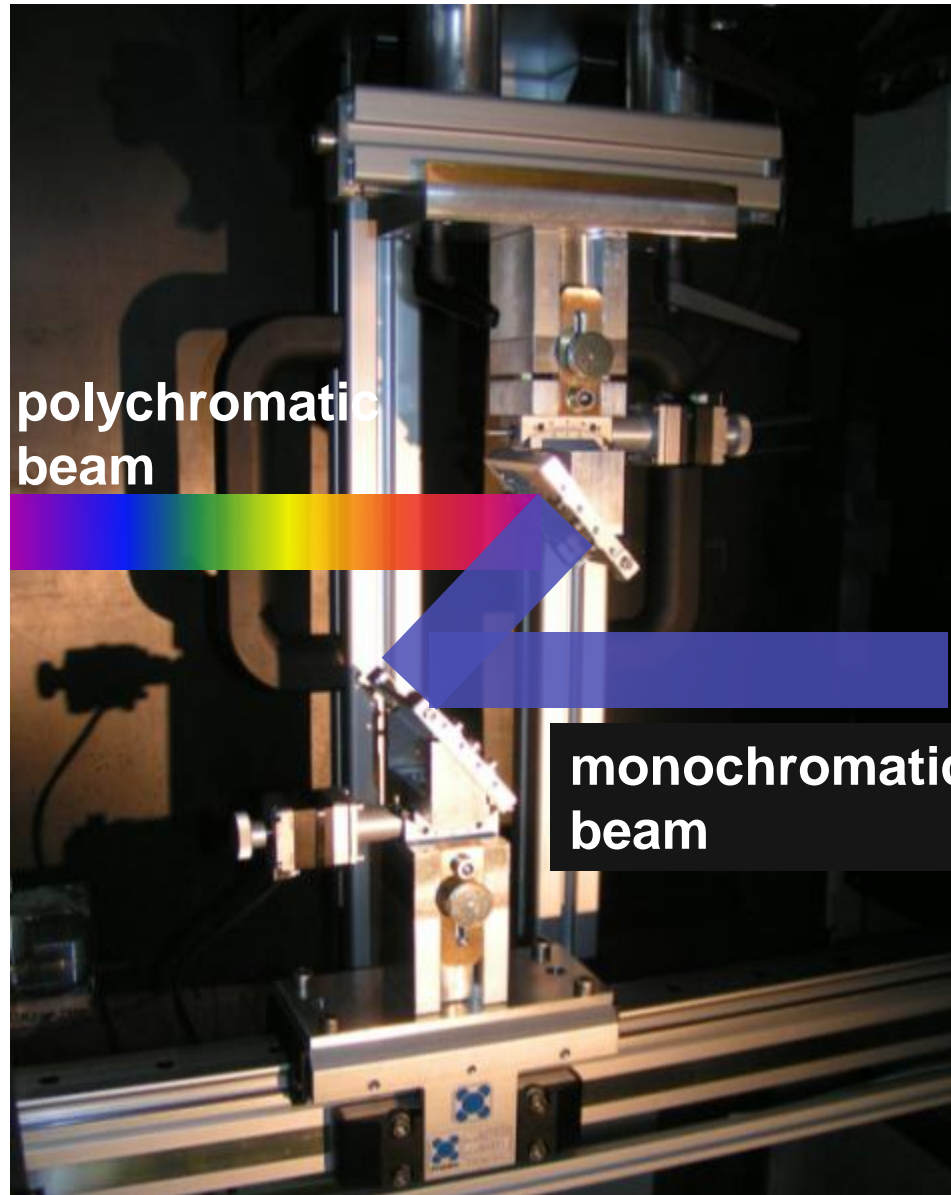
Double crystal monochromator:
PCG crystals (mosaicity of 0.8°)

Range: $2.0 - 6.5 \text{ \AA}$

Resolution ($\Delta\lambda/\lambda$): $\sim 3\%$

Neutron flux: $\sim 4 \times 10^5 \text{ n/cm}^2\text{s}$
(at $\lambda=3.0 \text{ \AA}$)

Beam size: $5 \times 20 \text{ cm}^2$



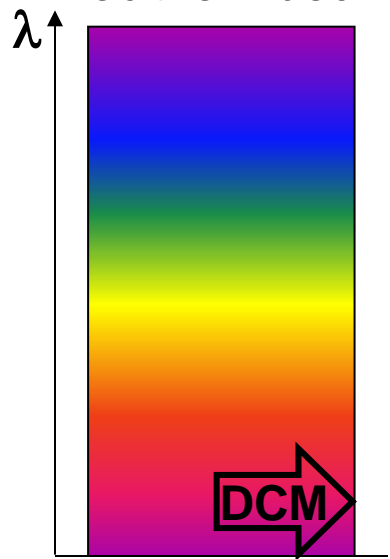
Kardjilov, Nikolay, et al. "New trends in neutron imaging." *Nuclear Instruments and Methods in Physics Research Section A: Accelerators, Spectrometers, Detectors and Associated Equipment* 605.1 (2009): 13-15.



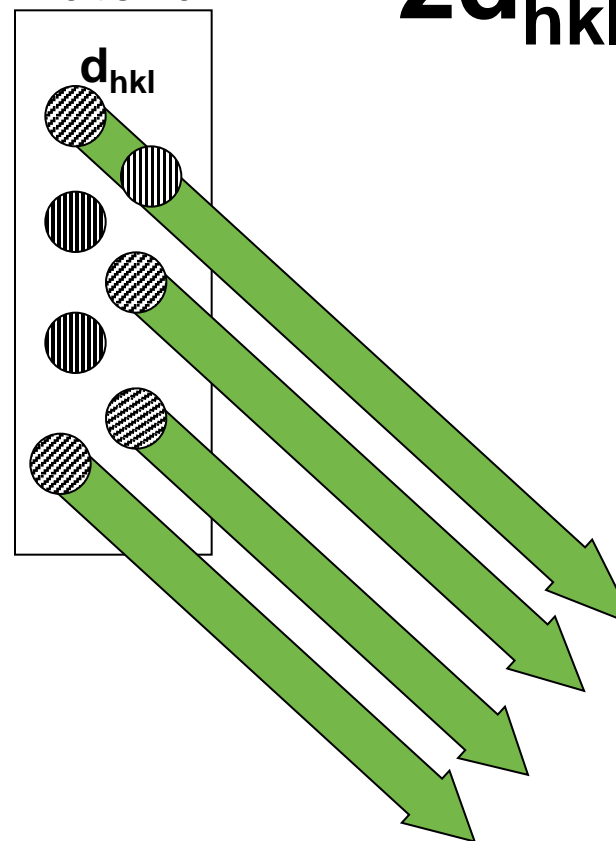
Diffraction Contrast

Coherent scattering – Bragg edges

polychromatic
neutron beam



polycrystalline
material



Bragg's law

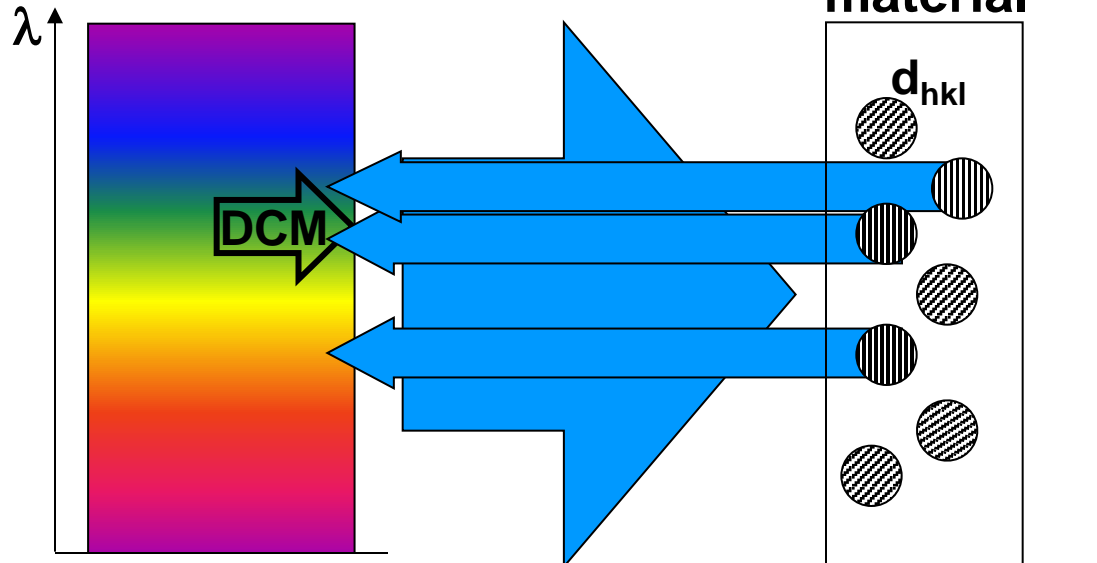
$$2d_{hkl} \sin\theta = \lambda$$



Diffraction Contrast

Coherent scattering – Bragg edges

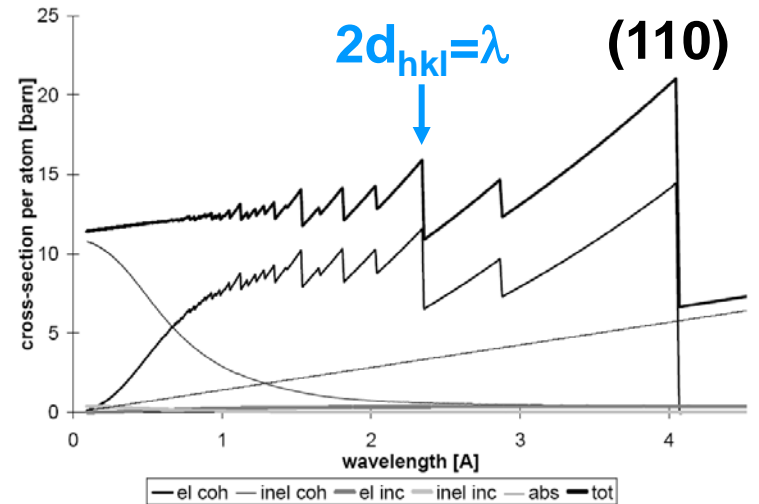
polychromatic neutron beam



Bragg's law

$$2d_{hkl} \sin 90^\circ = \lambda$$

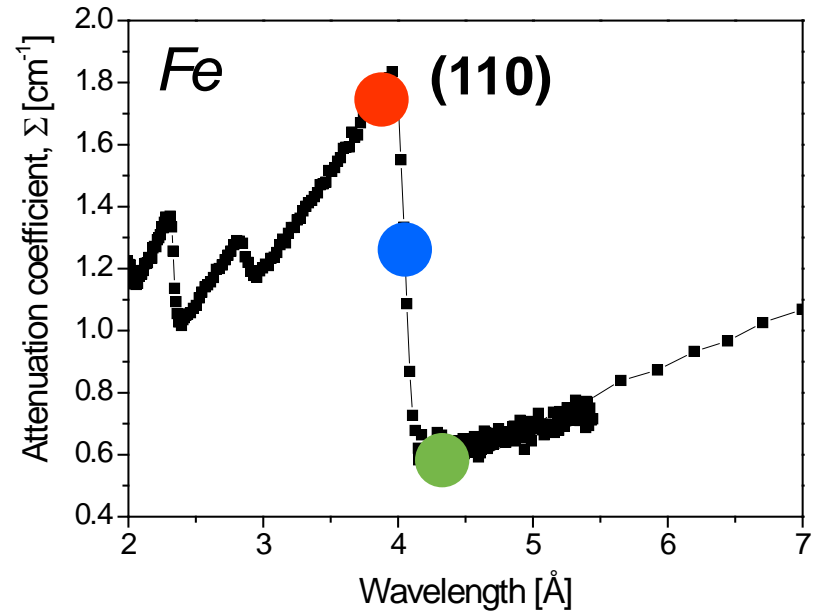
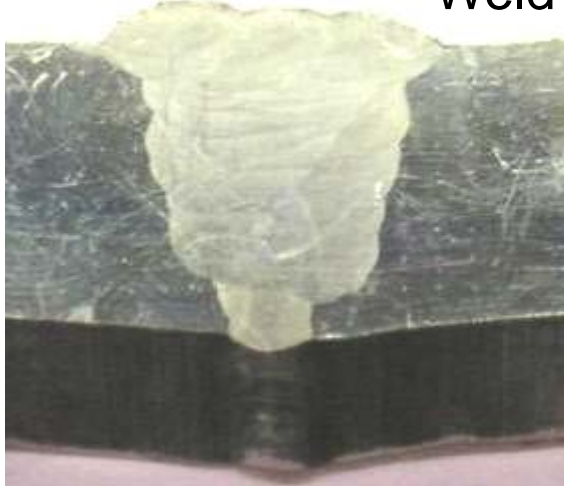
Cross-sections of iron per atom



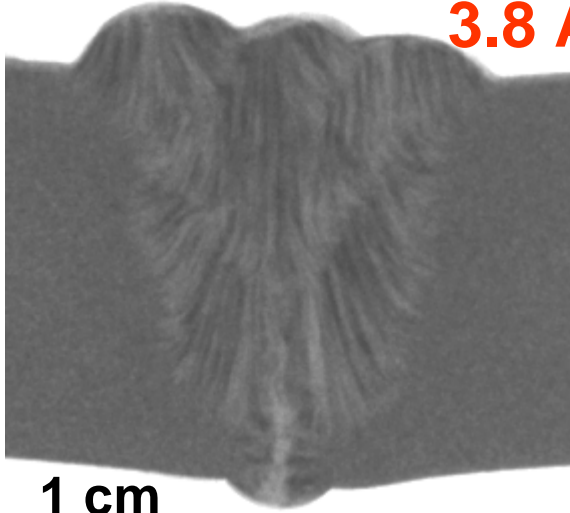
Neutron imaging

Energy-selective radiography

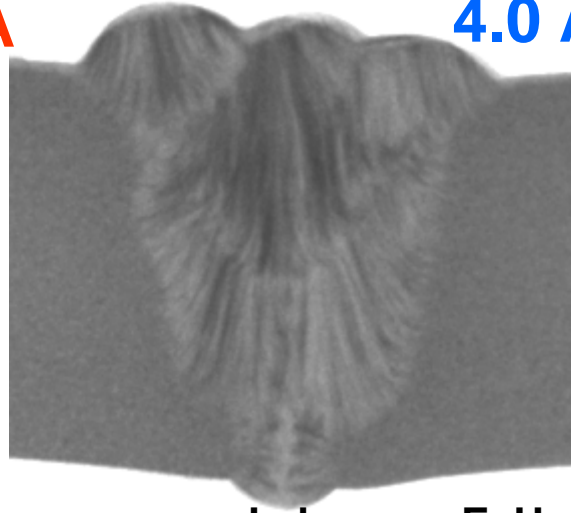
Weld (photo)



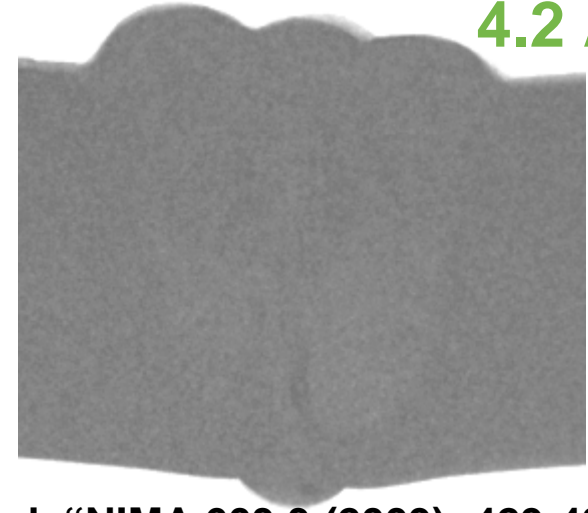
3.8 \AA



4.0 \AA

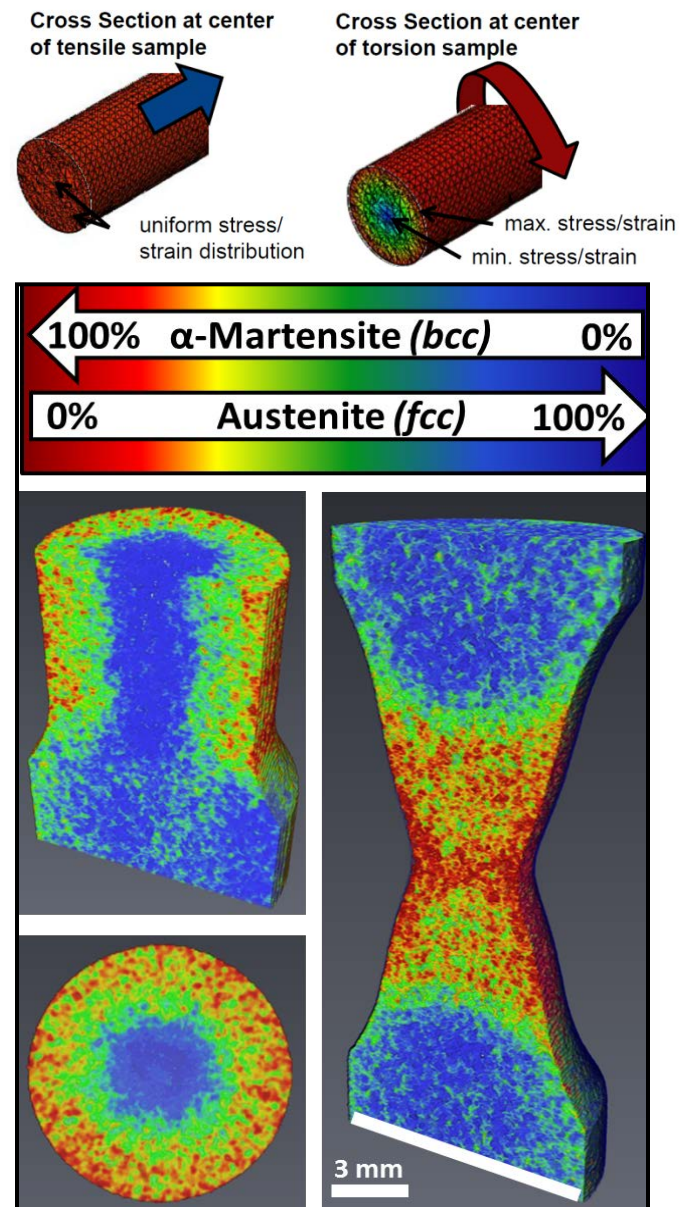
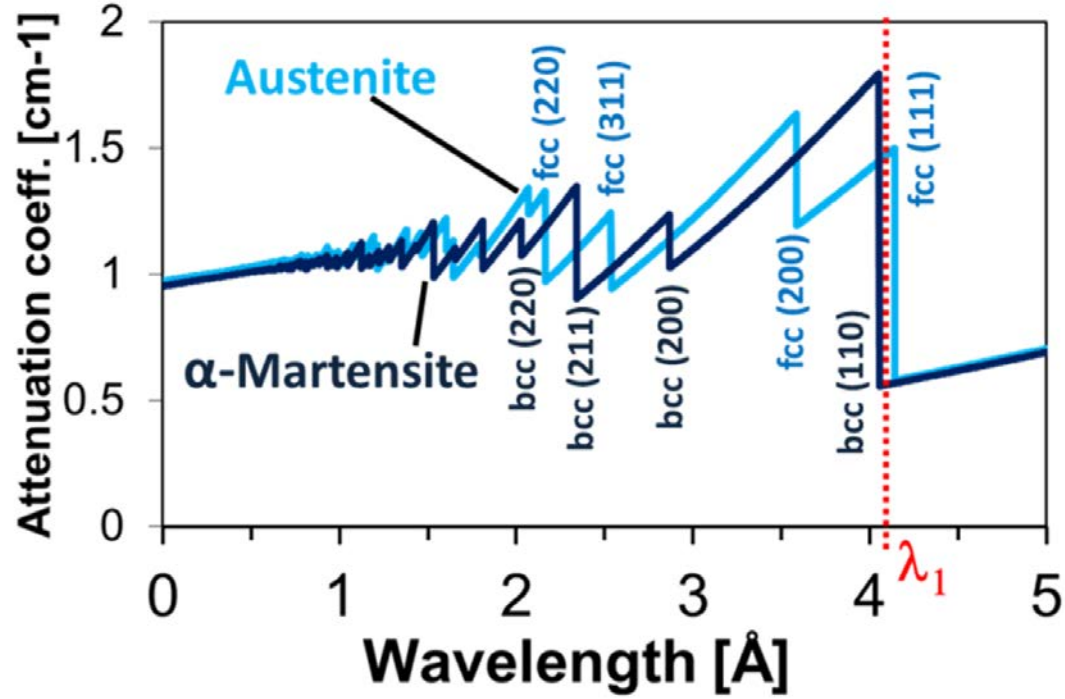


4.2 \AA



Lehmann, E. H., et al. "NIMA 603.3 (2009): 429-438.

3D Phase mapping in metals



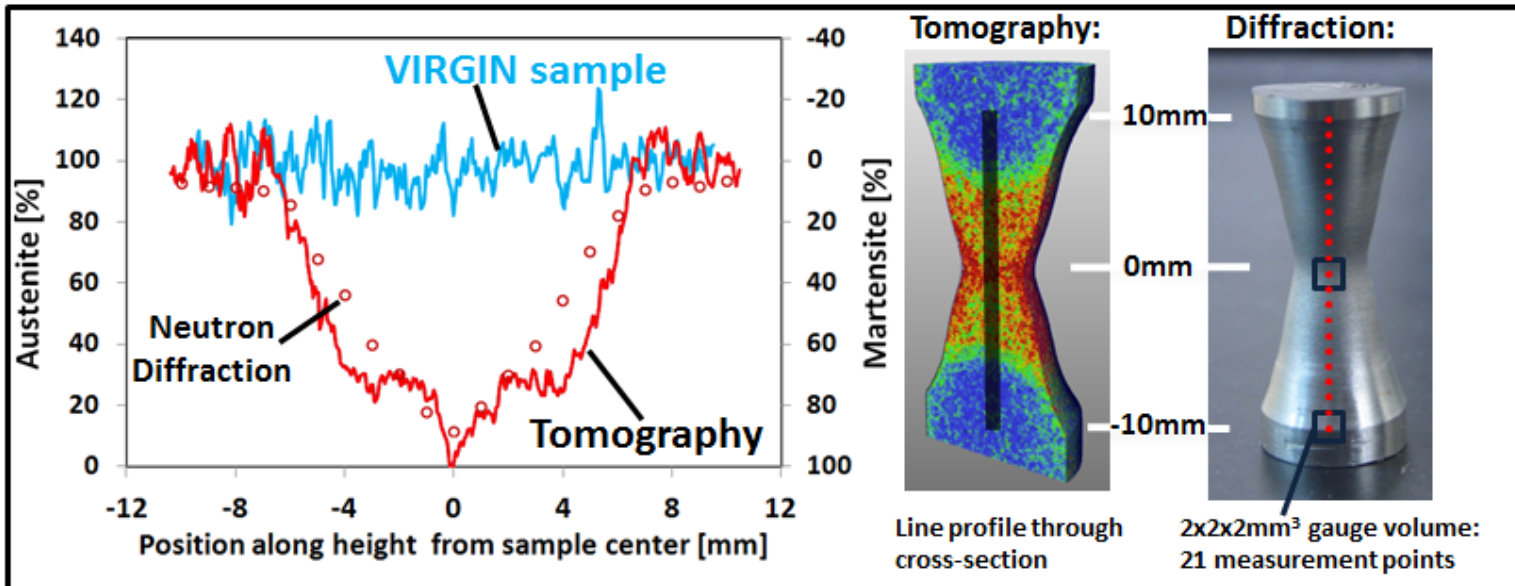
Energy-selective neutron tomography of TRIP-steel

R. Woracek et al., Advanced Materials 26 (2014)

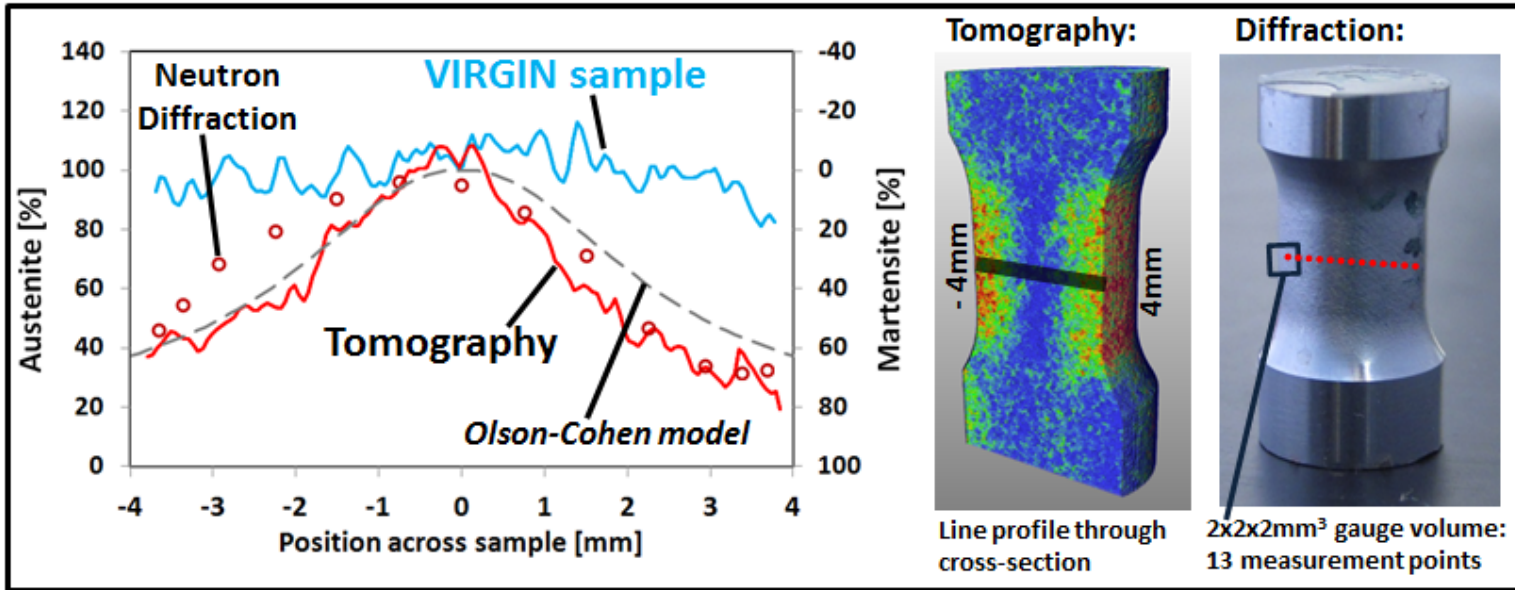
N. Kardjilov, Oxford School on Neutron Scattering, 11. September 2019

Diffraction Contrast

Tensile sample



Torsion sample



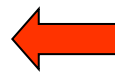


Resolution

- Beam optimisation
- Detector development

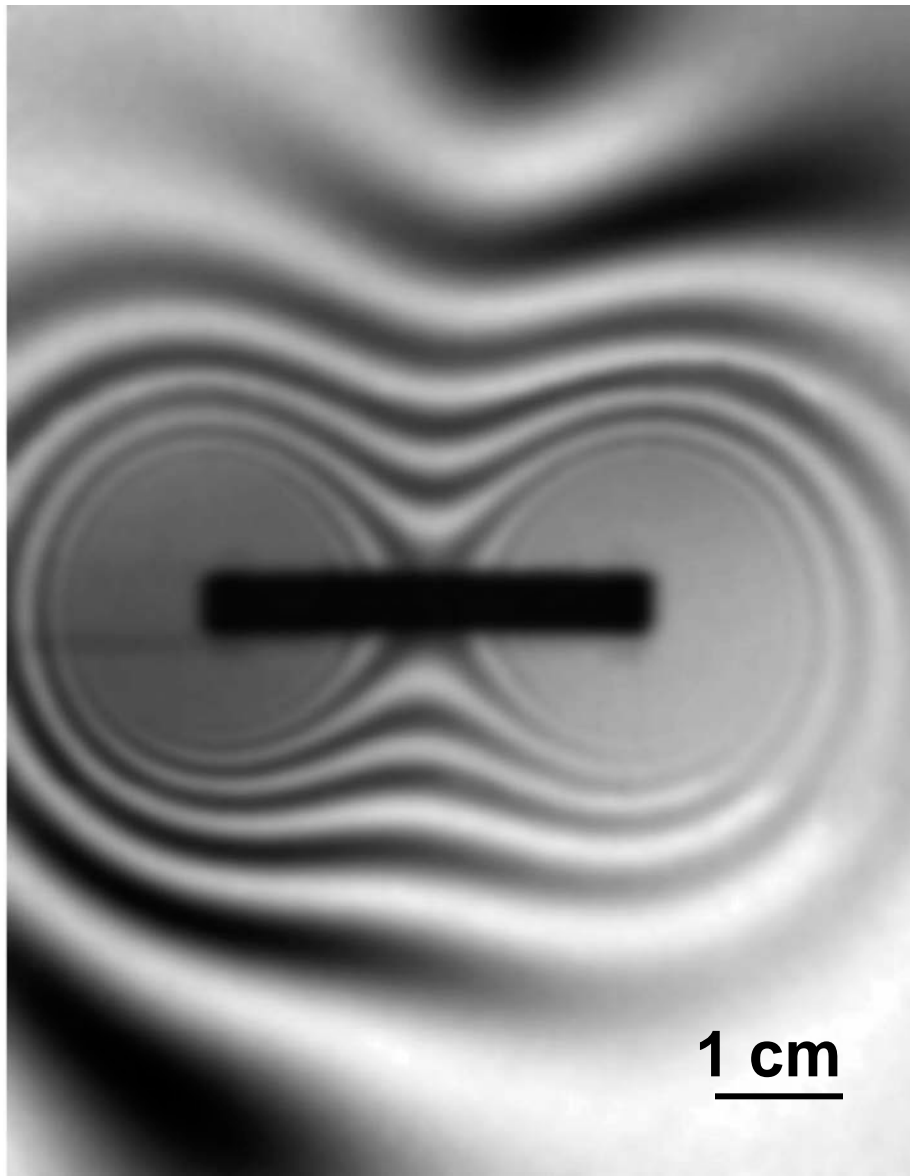
Contrast

- Neutron interaction with matter
 - n - absorption
 -  - scattering
 -  - magnetic interaction



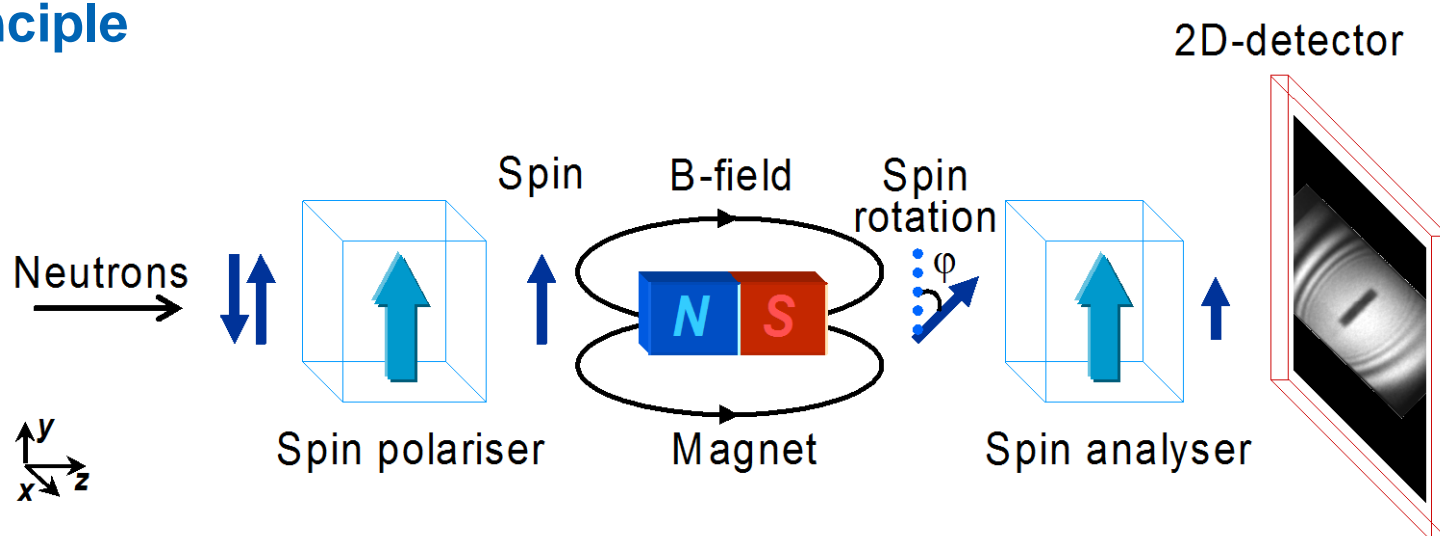


Magnetic Contrast



Magnetic Contrast

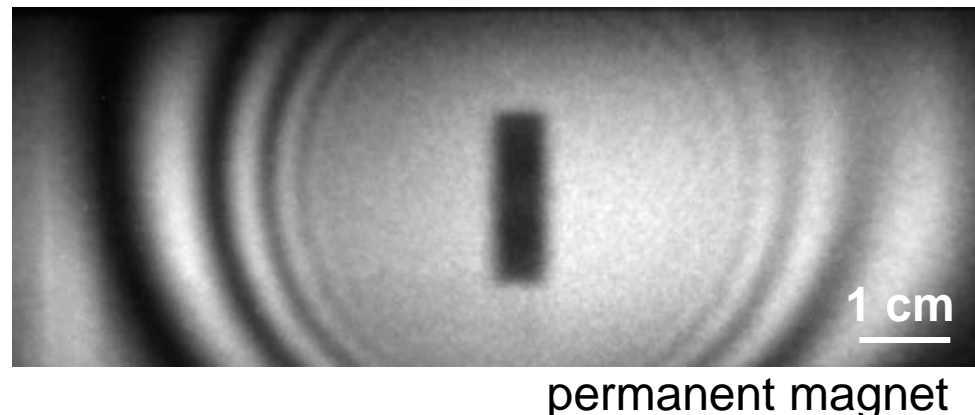
Principle



$$\varphi = \omega_L t = \frac{\gamma_L}{v} \int_{path} H ds$$

Experimental parameters

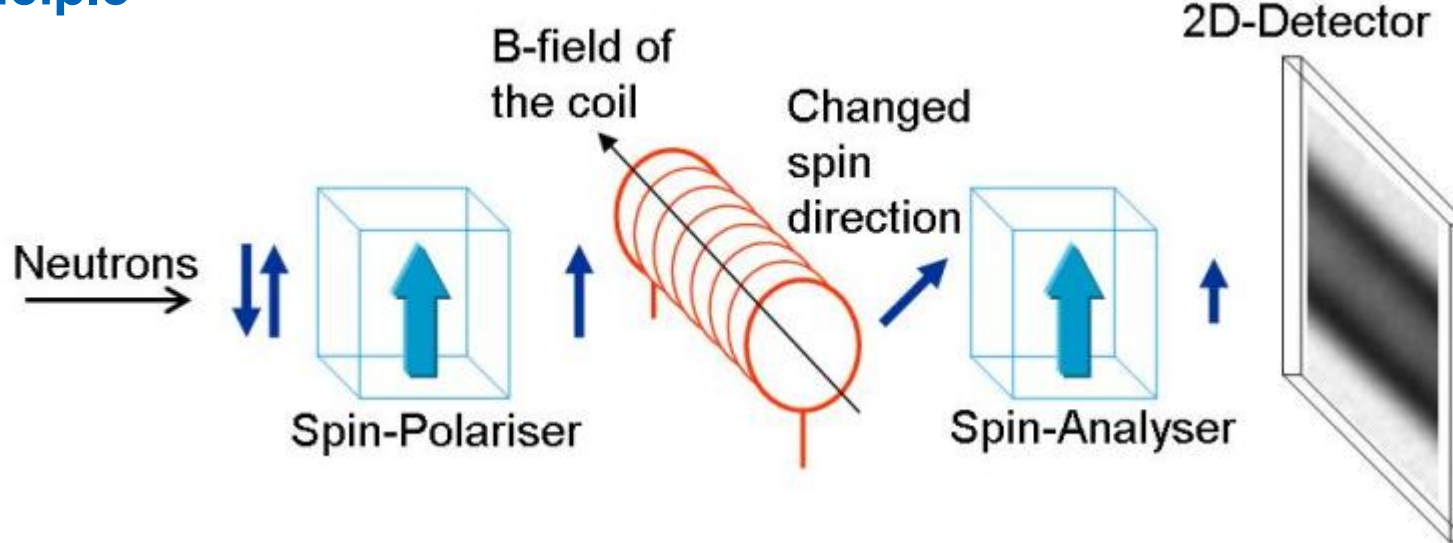
- Solid state polarizing benders
- Beam size (WxH): 20 x 4 cm²
- Exposure times: ~10 min / image



N. Kardjilov et al, Nature Physics 4, 399, (2008)

Magnetic Contrast

Principle

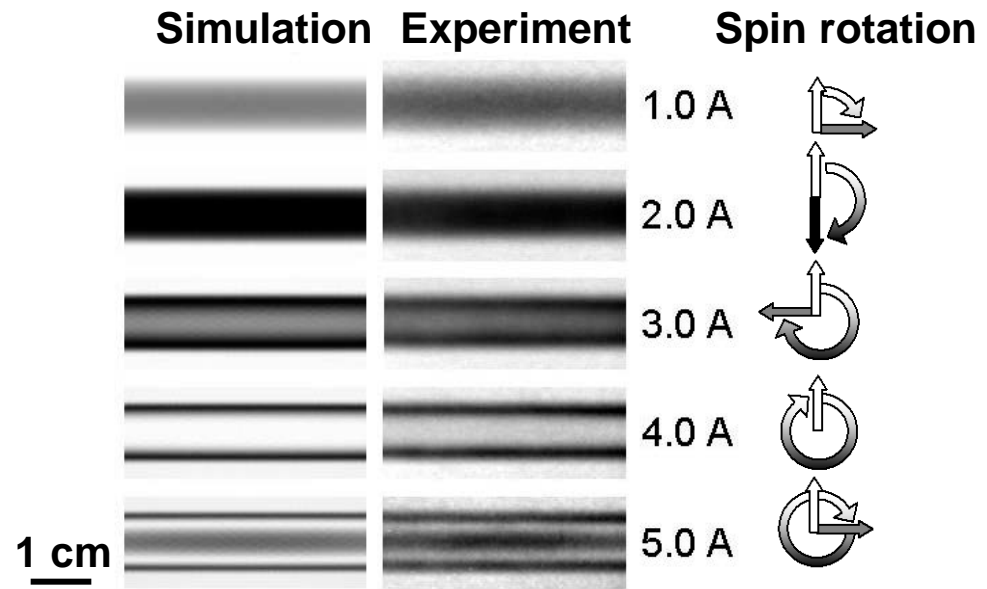


Biot-Savart law

$$d\vec{B} = \frac{\mu_0}{4\pi} \frac{Id\vec{l} \times \hat{r}}{r^2}$$

Spin rotation

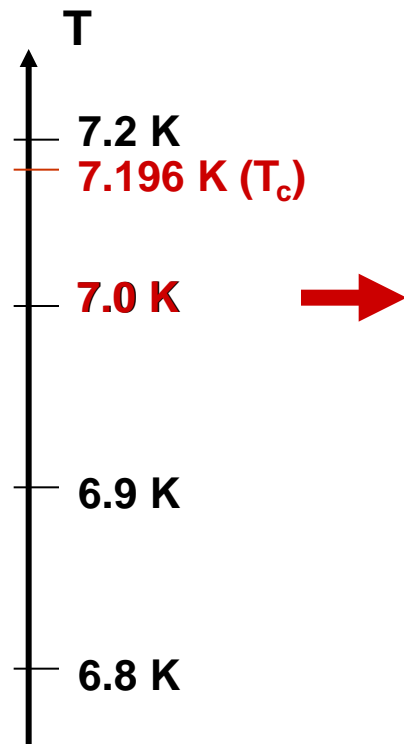
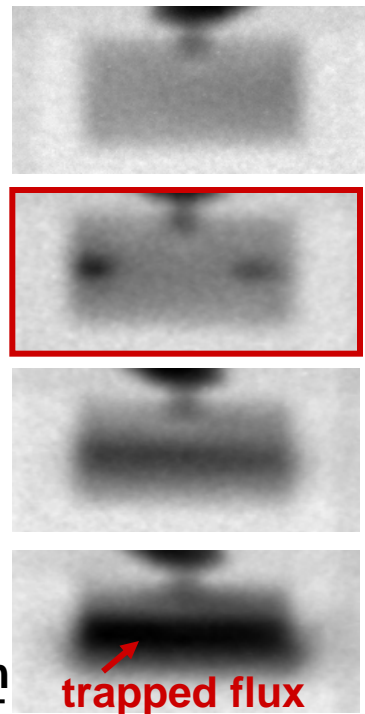
$$\varphi = \frac{\gamma_L}{v} \int_{path} B ds$$



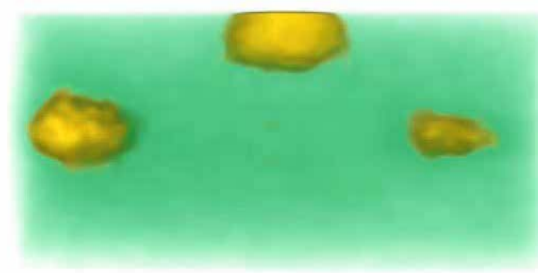
Magnetic Contrast

Example: Flux pinning

Pb cylinder
(polycrystalline)



Tomography

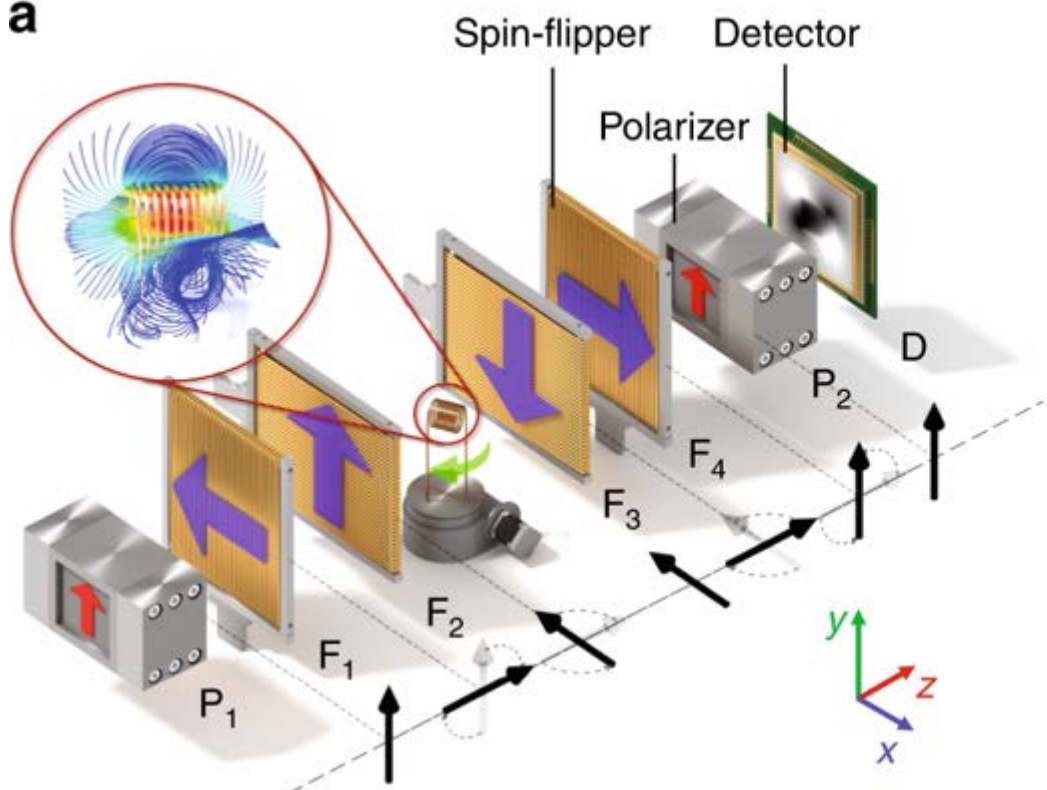


Flux pinning at cooling down below T_c while applying a homogenous magnetic field of 10 mT perpendicular to the beam.

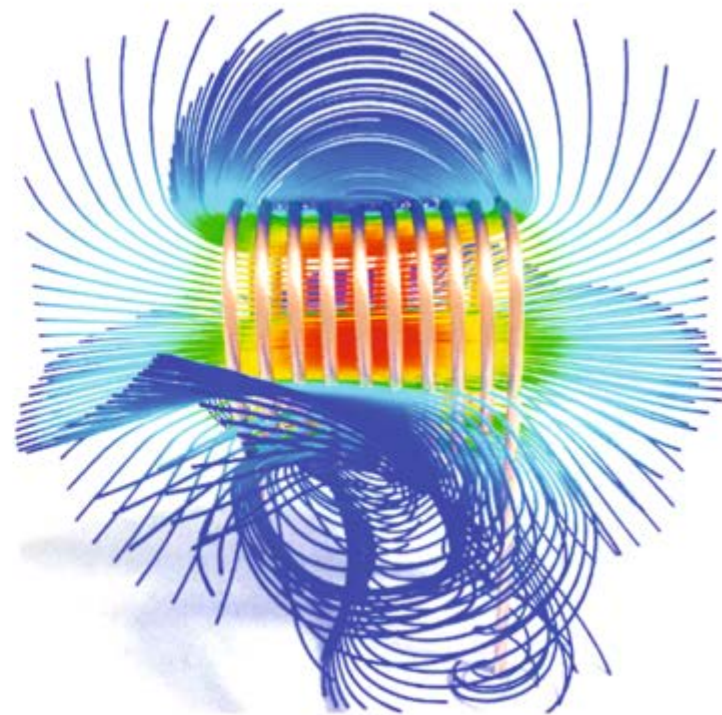
The images were recorded after switching off the magnetic field.

Experimental setup

a



b



Tensor tomography. **a** Schematic drawing of the setup used for tensor tomography with spin-polarized neutrons, comprising spin polarizers (P), spin flippers (F) and a detector (D). **b** Selected magnetic field lines around an electric coil (calculation)

A. Hilger, et al, Nature Communications 9.1 (2018): 4023



Magnetic Contrast

Analysis of Spin component:

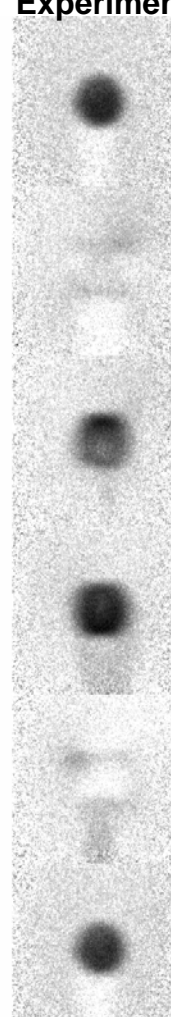
X

Y

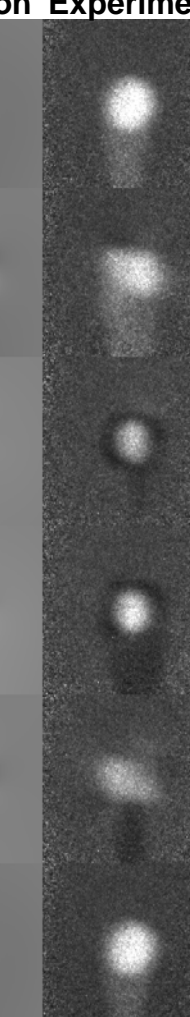
Z

Rotation angle
of the sample: 0°

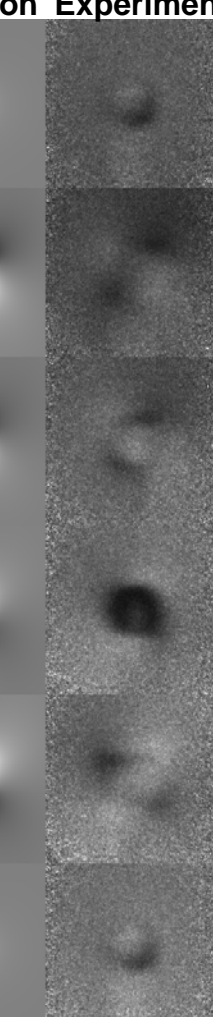
Simulation Experiment



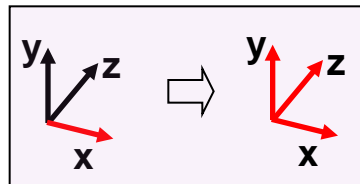
Simulation Experiment



Simulation Experiment



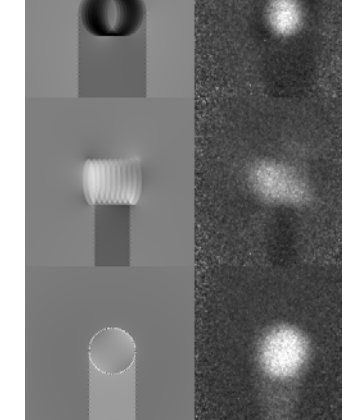
Initial spin direction: X



216°



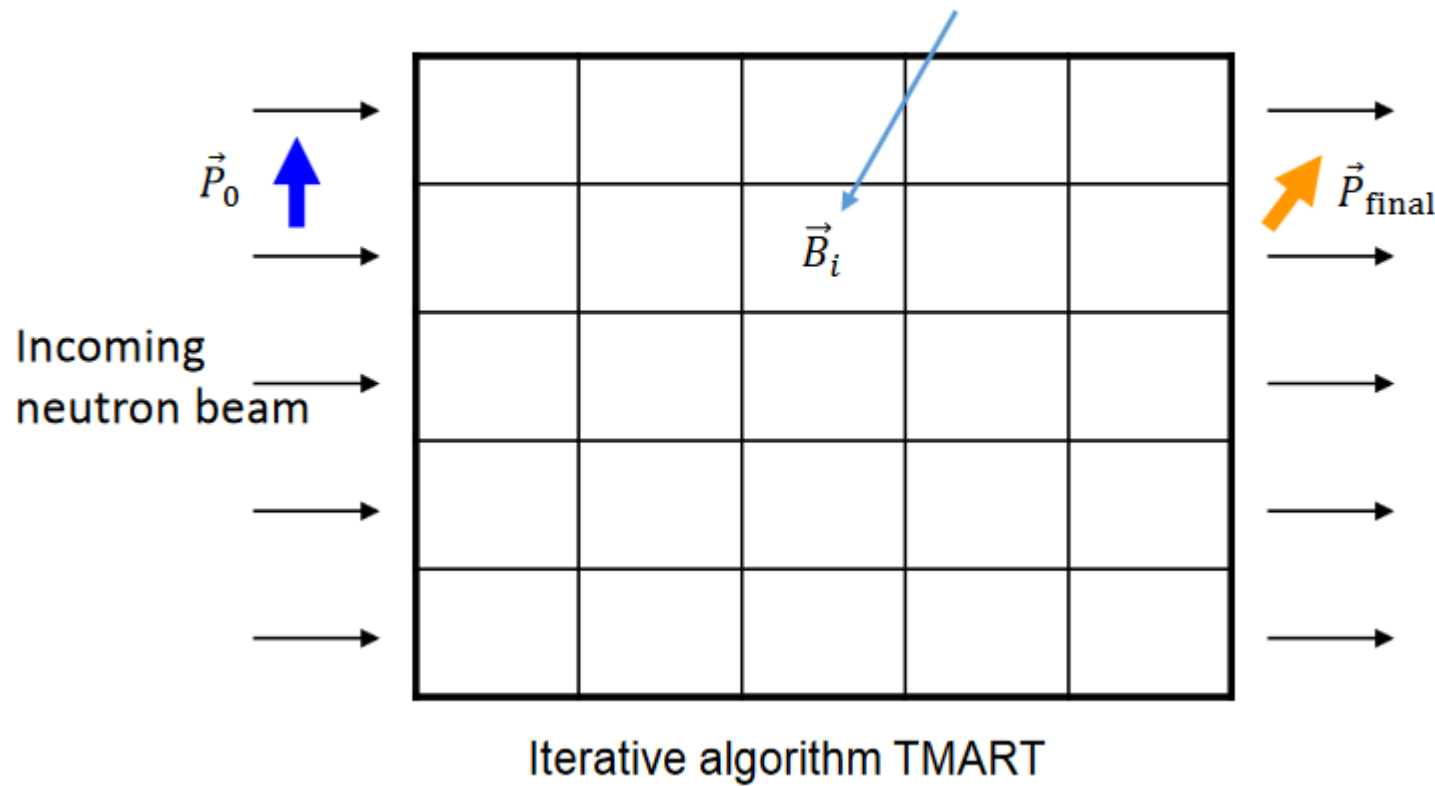
288°



360°



Magnetic vector field \vec{B}_i in volume element α_i



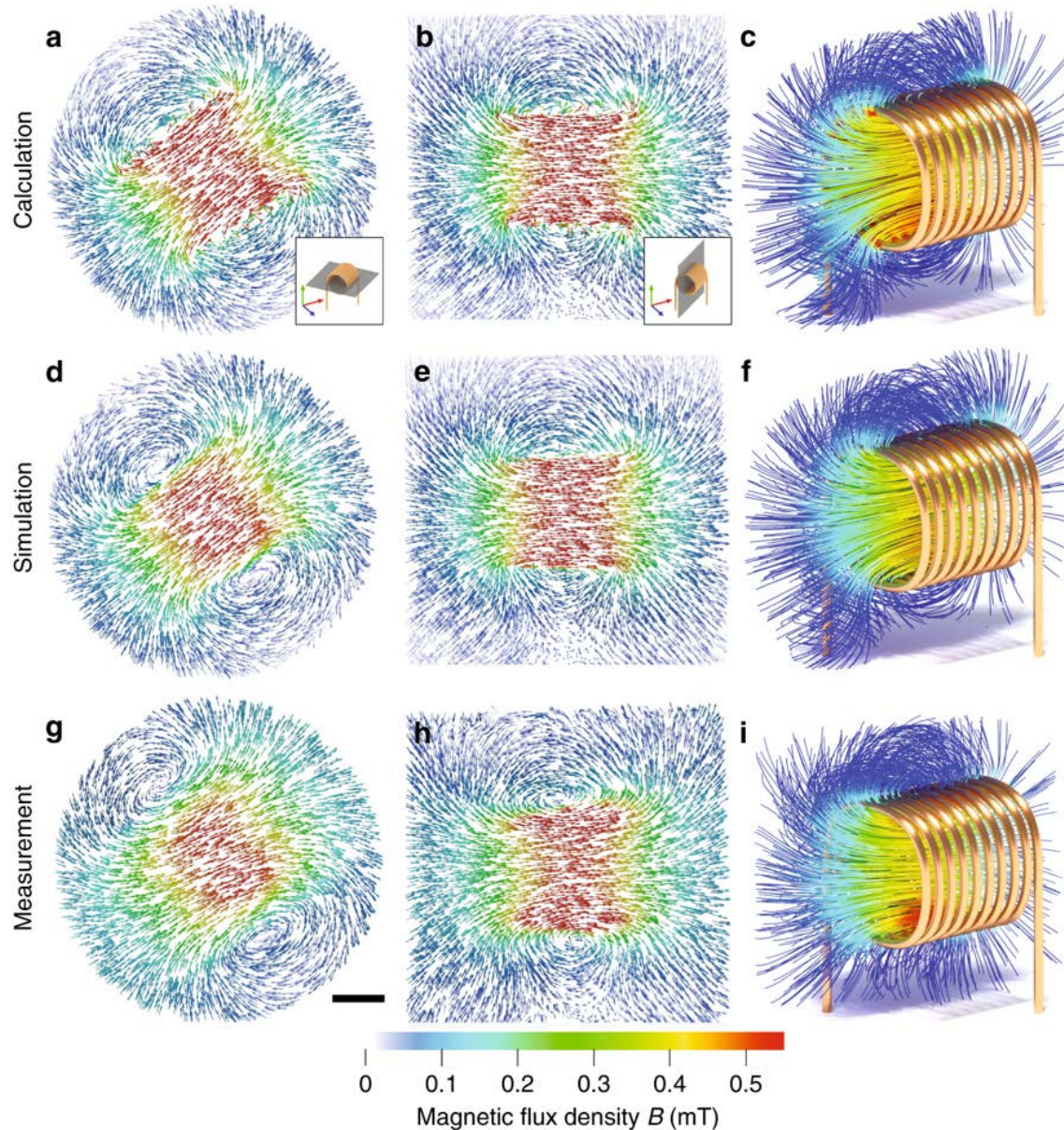
$$T_{\text{final}}(\vec{n}, \alpha) = T(\vec{n}_N, \alpha_N) \cdot \dots \cdot T(\vec{n}_i, \alpha_i) \cdot \dots \cdot T(\vec{n}_1, \alpha_1) = \prod_{i=N}^1 T(\vec{n}_i, \alpha_i).$$

$$\vec{P}_{\text{final}} = T_{\text{final}}(\vec{n}, \alpha) \cdot \vec{P}_0.$$

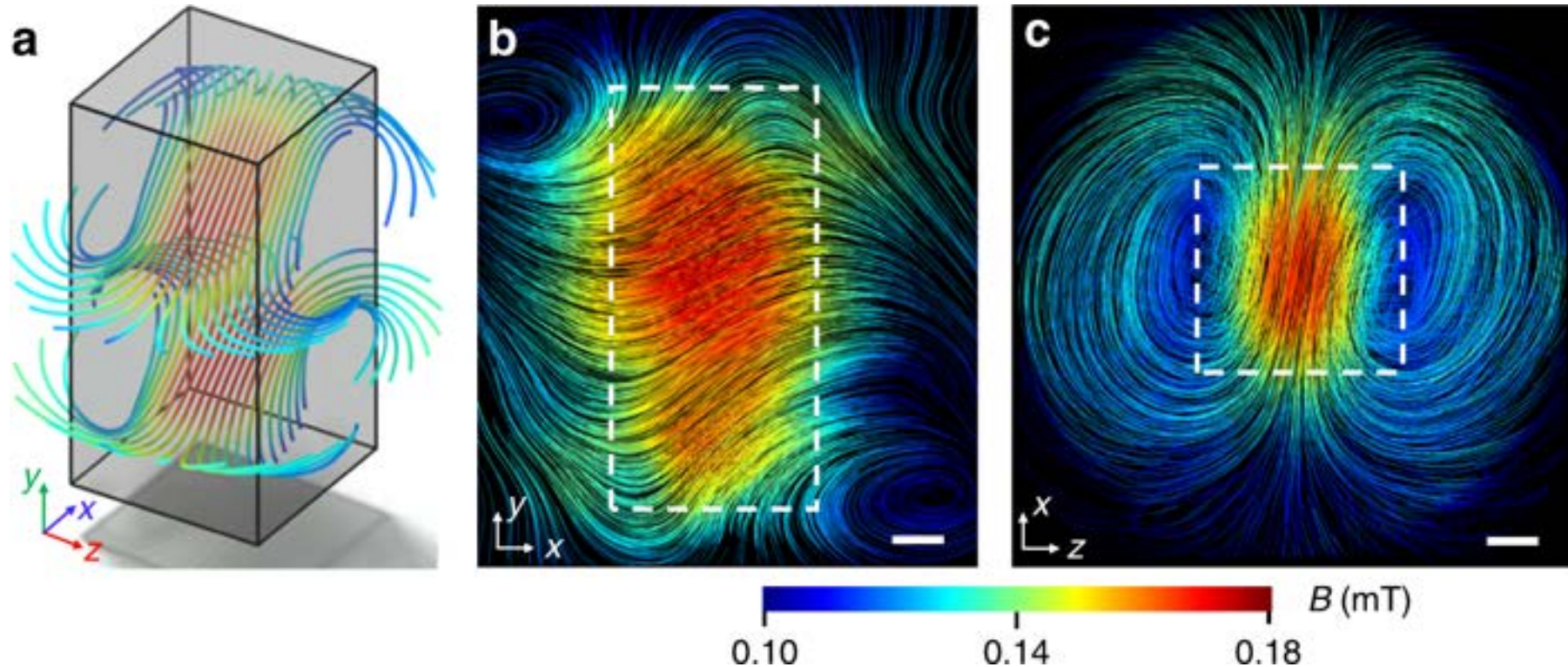
A. Hilger, et al, Nature Communications 9.1 (2018): 4023



Tensorial reconstruction

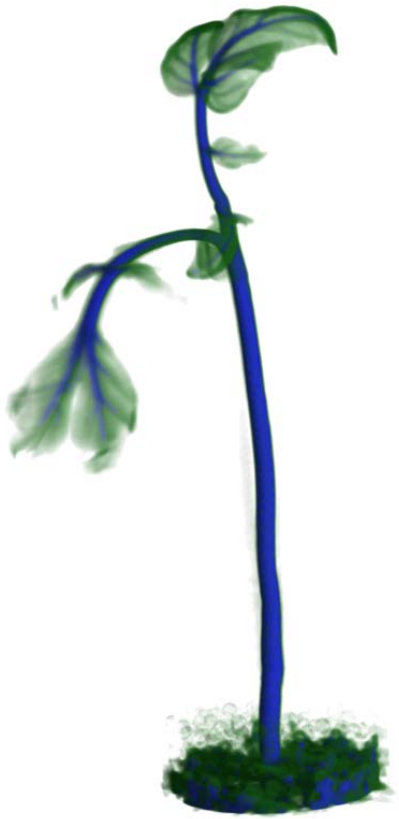


Quantitative magnetic tomography



Magnetic vector field inside a superconducting lead sample measured at $T = 4.3\text{ K}$.
a Some selected magnetic field lines show the location of the magnetic field inside the sample indicated by the cuboid. **b** Magnetic field lines in a selected xy plane (silhouette of the lead sample marked by dotted lines). Scale bar, 5 mm. **c** Magnetic field lines in a selected xz plane. Scale bar, 5 mm.

A. Hilger, et al, Nature Communications 9.1 (2018): 4023



Thank you !

https://www.helmholtz-berlin.de/user/user-info/user-offices/neutrons/index_en.html